

1 Changes in sea ice cover and ice sheet extent at the Yermak Plateau during the last 160 ka –

2 Reconstructions from biomarker records.

3

4 Kremer, A., Stein, R., Fahl, K., Ji, Z., Yang, Z., Wiers, S., Matthiessen, J., Forwick, M.,

5 Löwemark, L., O'Regan, M., Chen, J., Snowball, I.

6

7

8

9

10

11

12

13

14

15

16

17

18

19

20

21

22

23

24

25

26 Abstract

27

28 The Yermak Plateau is located north of Svalbard at the entrance to the Arctic Ocean, i.e. in an
29 area highly sensitive to climate change. A multi proxy approach was carried out on Core
30 PS92/039-2 to study glacial-interglacial environmental changes at the northern Barents Sea
31 margin during the last 160 ka. The main emphasis was on the reconstruction of sea ice cover,
32 based on the sea ice proxy IP_{25} and the related phytoplankton - sea ice index PIP_{25} . Sea ice was
33 present most of the time but showed significant temporal variability decisively affected by
34 movements of the Svalbard Barents Sea Ice Sheet. For the first time, we prove the occurrence of
35 seasonal sea ice at the eastern Yermak Plateau during glacial intervals, probably steered by a
36 major northward advance of the ice sheet and the formation of a coastal polynya in front of it.
37 Maximum accumulation of terrigenous organic carbon, IP_{25} and the phytoplankton biomarkers
38 (brassicasterol, dinosterol, HBI III) can be correlated to distinct deglaciation events. More
39 severe, but variable sea ice cover prevailed at the Yermak Plateau during interglacials. The
40 general proximity to the sea ice margin is further indicated by biomarker (GDGT) - based sea
41 surface temperatures below 2.5°C .

42

43

44

45

46

47

48

49

50

51 1. Introduction

52

53 The decline of Arctic sea ice began to draw attention in 2005, when summer sea ice reached the
54 lowest extent since satellite based observations started in 1979 (Serreze et al., 2007). Having
55 enlivened the debate around anthropogenic climate change, this dramatic trend continued -
56 much faster than forecast - when a new record low in sea ice extent was reached in 2007
57 followed by another in 2012 (Comiso et al., 2008; Parkinson and Comiso, 2013). Most recently,
58 the maximum winter extent of Arctic sea ice reached a record minimum in 2016 (National Snow
59 & Ice Data Center, <https://nsidc.org>). Playing a crucial role in maintaining climatic stability
60 worldwide, such a development of Arctic sea ice is alarming, even more when polar amplification
61 of global warming is taken into account (Serreze and Barry, 2011). Arctic sea ice impacts the
62 Earth's global energy budget through regulating the surface albedo, controls the exchange of
63 heat and moisture between the atmosphere and the ocean, contributes to global heat transfer
64 and influences local primary production (Broecker, 1997; Hall, 2004; Dieckmann and Hellmer,
65 2008). Despite this fundamental relevance of Arctic sea ice, our understanding of its interaction
66 with different internal and external forces is still incomplete for certain regions and timespans. In
67 order to improve climate predictions and related measures, it is essential to know how this
68 sensitive system responds to climatic variations. To evaluate the anthropogenic impact on sea
69 ice decline, it is imperative to extend records of past sea ice extent beyond the modern
70 observational period.

71 The Yermak Plateau north of Svalbard is located at the interface between the Arctic Ocean and
72 the Atlantic Ocean. This area is subject to a range of environmental forces, e.g., the intensity of
73 various ocean currents and the glaciation on Svalbard. Throughout the late Quaternary, the
74 Svalbard Barents Sea Ice Sheet (SBIS) advanced several times towards the shelf break along
75 western and northern Svalbard, strongly impacting oceanic conditions and sedimentation

76 regimes (e.g., Svendsen et al., 2004; Winkelmann et al., 2008a; Knies et al., 2009; Jessen et al.,
77 2010). According to the glaciation model of Mangerud et al. (1998), four major ice sheets built up
78 and decayed along western Svalbard during the last 150 ka: the most extensive one during the
79 late Saalian (>140 ka), followed by an early (~110 ka), a middle (60 ka) and a late Weichselian
80 glaciation (~20 ka; Landvik et al., 1998; Mangerud et al., 1998; Hughes et al., 2016). The
81 northernmost extent as well as local discrepancies are, however, still under debate and need
82 further investigation (Winkelmann et al., 2008a; Clark et al., 2009; Ingolfsson and Landvik, 2013;
83 Landvik et al., 2013). Intensified Atlantic Water (AW) advection via the West Spitsbergen Current
84 (WSC) and related open water areas in the Greenland, Iceland and Norwegian Seas are
85 believed to be an important trigger for ice sheet growth by providing extensive amounts of
86 moisture (Hebbeln et al., 1994; Dokken and Hald, 1996). The strongest inflow of warm AW was
87 recorded for the Eemian and the Holocene (Henrich, 1998; Knies et al., 1999; Matthiessen et al.,
88 2001; Matthiessen and Knies, 2001; Wollenburg et al., 2001; Spielhagen et al., 2004). Less
89 pronounced advection was observed for MIS 5c, 5a and 3, while the glacial periods MIS 6, 4 and
90 2 were characterised by persistent but modified (temperate) inflow (Henrich, 1998; Knies et al.,
91 1999).

92 The main objective of the current study is to reconstruct sea ice variability in the northernmost
93 Fram Strait related to late Quaternary glacial-interglacial cycles. For this purpose, measurements
94 of specific biomarkers were carried out on Core PS92/039-2 from the Yermak Plateau north of
95 Svalbard. Supplemented by a set of organic and sedimentological parameters (lithology, IRD,
96 TOC, C/N ratio), these biomarker data provide a solid base to outline the environmental
97 development of the Fram Strait during the last 160 ka.

98

99 2. Biomarker proxies used for paleoenvironmental reconstruction in this study

100

101 The organic-geochemical investigation of marine archives with regard to specific molecular
102 signatures (biomarkers) has been a common practice in paleoenvironmental studies for some
103 time (e.g., Meyers, 1997; Stein and Macdonald, 2004; Volkman, 2006; Eglinton and Eglinton,
104 2008; Sachs et al., 2013). In this study, the main focus is on the reconstruction of past sea ice
105 cover, with estimates of the sea surface temperature (SST) serving as additional verification.
106 Furthermore, the production of marine, open-water phytoplankton (hereafter referred to as
107 “phytoplankton”) and the input of terrigenous material are assessed using specific biomarkers.
108 In the past decade, the novel sea ice proxy IP_{25} (C_{25} HBI [highly branched isoprenoid] monoene
109 = IP_{25} ; Belt et al., 2007) paved the way for reconstructing the variability of past sea ice conditions
110 in the Arctic realm, reaching back to the late Miocene (Stein et al., 2016). Biosynthesised by
111 diatoms exclusively living in Arctic sea ice (Belt et al., 2008; Brown et al., 2014), the
112 presence/absence of this organic molecule in sediment samples serves as a presence/absence
113 indicator for spring sea ice cover (Belt et al., 2007). An even more reliable estimate of sea ice
114 conditions is achieved when combining IP_{25} with phytoplankton biomarkers, creating the PIP_{25}
115 index (phytoplankton marker – IP_{25} = PIP_{25} ; Müller et al., 2011). In this way, the problem of
116 misjudging absent IP_{25} , either reflecting perennial ice cover or ice-free water, can be
117 circumvented.

118 Although the principle of this approach is convincing, existing limitations should be considered
119 when using PIP_{25} for sea ice reconstructions. Difficulties may arise when in-phase fluxes of the
120 phytoplankton marker and IP_{25} occur (Müller et al., 2011). In this case, coevally low (indicating
121 permanent sea ice conditions) or high (indicating marginal sea ice conditions) input would result
122 in similar PIP_{25} values and a misleading sea ice evaluation. Therefore, it is key to always
123 consider the individual biomarker profiles alongside the PIP_{25} record. The sterols brassicasterol
124 and dinosterol are commonly used as phytoplankton markers in the PIP_{25} (P_BIP_{25} and P_DIP_{25} ,
125 respectively) calculation. As these sterols are biosynthesised by a relatively broad group of

126 marine phytoplankton, mainly diatoms and dinoflagellates (Boon et al., 1979; Robinson et al.,
127 1984; Volkman et al., 1998), their sedimentary signal represents various environmental
128 conditions. Further, the PIP₂₅-based sea ice reconstructions may be biased by selective
129 biomarker degradation of the structurally differing IP₂₅ and sterol compounds (for a detailed
130 review of potential limitations of the PIP₂₅ approach, see Stein et al., 2012; Navarro-Rodriguez et
131 al., 2013; Belt and Müller, 2013).

132 Despite potential limitations, both P_BIP₂₅ and P_DIP₂₅ indices show a positive correlation with
133 modern satellite-based sea ice observations (Müller et al., 2012; Xiao et al., 2015a) and have
134 been used to define paleo sea ice conditions more quantitatively in a variety of studies (e.g.,
135 Müller et al., 2012; Stein and Fahl, 2013; Müller and Stein, 2014; Belt et al., 2015; Xiao et al.,
136 2015b; Hörner et al., 2016; Stein et al., 2017a).

137 Nonetheless, the adoption of a more suitable open water counterpart to IP₂₅ is recently
138 investigated with special attention to a tri-unsaturated HBI lipid (HBI III, Belt et al., 2000; Belt et
139 al., 2015; Smik et al., 2016). The HBI III compound is found in marine sediments of temperate
140 regions worldwide but is especially enriched within the Marginal Ice Zone (MIZ; transition
141 between open ocean and sea ice) of the Arctic Ocean (Belt et al., 2000, 2015). Even though the
142 specific source of this compound is not identified unequivocally, the only known producers are
143 marine diatoms (Belt et al., 2000; Rowland et al., 2001). The concentrations of IP₂₅ and HBI III
144 are much closer in magnitude than IP₂₅ and brassicasterol or dinosterol, potentially superseding
145 the need of the concentration balance factor currently used in the PIP₂₅ quantification (Belt et al.,
146 2015; Smik et al., 2016; see also “Material and methods”). The P_{III}IP₂₅ approach already enabled
147 reliable paleo sea ice reconstructions by Belt et al. (2015), Berben et al. (2017) and Stein et al.
148 (2017b). However, the applicability of this approach needs to be evaluated by further analysis of
149 downcore records and the correlation of surface data sets to satellite-derived sea ice
150 observations.

151 For temperature reconstruction, the alkenone - based U_{37}^k index (Brassell et al., 1986; Prahl and
152 Wakeham, 1987) and the GDGT (glycerol dialkyl glycerol tetraether) - based TEX_{86} index
153 (Schouten et al., 2002) are two common organic-geochemical tools in paleoceanographic
154 studies. While correlating well with SSTs in tropical and temperate regions, these approaches
155 show large inaccuracies in regions dominated by colder water masses (Kim et al., 2008). The
156 modified TEX_{86}^L index for temperatures below 15°C (Kim et al., 2010) yields a better correlation
157 but still anomalously high temperatures for the Arctic Ocean (Ho et al., 2014). Liu et al. (2012)
158 identified GDGTs with an additional hydroxyl group on the alkyl chain. These hydroxylated
159 GDGTs (OH-GDGTs) likely originate from planktonic archaea and are widespread in marine
160 surface and downcore sediments (Liu et al., 2012; Fietz et al., 2013). Both the relative
161 abundance of individual OH-GDGTs and the number of their cyclopentane rings vary with
162 temperature (Fietz et al., 2013), leading to the development of the ring index RI-OH (Lü et al.,
163 2015). The revised RI-OH' index includes specific OH-GDGTs more abundant in polar regions,
164 therefore possibly representing a promising tool for the reconstruction of temperatures in this
165 specific environment. This study will use the RI-OH' index for the first time to calculate polar
166 SSTs, thereby providing important information about its applicability in high latitudes.

167 For the source identification of organic matter in marine sediments, a variety of organic-
168 geochemical bulk parameters (e.g., C/N ratio, $\delta^{13}C_{org}$ values, Rock-Eval parameters) and
169 specific biomarkers (e.g., *n*-alkanes, sterols) can be applied (Meyers, 1997; Stein and
170 Macdonald, 2004). The signals given by these different proxies may vary, however, when used
171 in combination, a solid evaluation of the relative proportions of marine and terrigenous organic
172 matter can be attained (e.g., Fahl and Stein, 2007; Volkman et al., 2008). To infer contributions
173 of terrigenous material, this study concentrated on the sterols β -sitosterol and campesterol
174 (Pryce, 1971; Huang and Meinschein, 1979). Although these biomarkers are found in a few
175 microalgae species, the main contributors are higher land plants (Volkman et al., 1986; Jaffé et

176 al., 1995; Rontani et al., 2014) that are delivered to the Arctic Ocean through Siberian river
177 runoff (Fahl et al., 2003; Fahl and Stein, 2007). In order to ensure the credibility of these results,
178 further proxies (i.e., C/N ratio, $\delta^{13}\text{C}_{\text{org}}$ values) were applied to trace terrigenous input
179 mechanisms.

180

181 3. Regional setting

182

183 The Yermak Plateau is located at the entrance to the Arctic Ocean off the north-western coast of
184 Svalbard (Fig. 1). To the west of the plateau, the Fram Strait, representing the northernmost
185 North Atlantic, displays the only deepwater connection between the Arctic Ocean and the world
186 oceans. Two major ocean current systems regulate the exchange of water masses in this
187 gateway, thereby generating an Atlantic and an Arctic domain: the WSC and the East Greenland
188 Current (EGC), respectively (Aagaard and Coachman, 1968; Aagaard, 1982). Steered by
189 bathymetry, the relatively warm WSC flows in intermediate depth northward along the western
190 continental margin of Svalbard (Bourke et al., 1988). Between 78 and 80°N, the WSC bifurcates
191 into an eastern (Svalbard) branch and a western (Yermak) branch (Aagaard et al., 1987; Manley
192 et al., 1992). The Svalbard Branch streams northeasterly, staying close to the continental margin
193 of Svalbard, and eventually enters the Arctic Ocean (Coachman & Aagaard, 1974; Aagaard et al.
194 1987; Manley, 1995). The Yermak Branch follows the western flank of the Yermak Plateau,
195 partly detaches from it north of 80°N, turns westward and recirculates southward as the Return
196 Atlantic Current (Bourke et al. 1988). Cold polar water and sea ice exit the Arctic Ocean along
197 the continental margin of East Greenland via the southward streaming EGC (Aagaard &
198 Coachman, 1968; Rudels et al., 1999). Positioned within the narrow MIZ, the study area is
199 subject to a pronounced seasonality. The formation of new sea ice is mainly restricted to the
200 autumn and winter months, while summer is the season of ice melt. When sea ice extent

201 reaches its maximum in March, the Svalbard Archipelago is usually largely enclosed by ice.
202 However, upwelling of relatively warm AW along the western and northern coast ensures ice free
203 conditions up to 80 - 82°N (Aagaard et al., 1987; Haugan, 1999; Ivanov et al., 2012). The
204 extension of these open water areas (polynyas) depends on the intensity of the WSC and shows
205 a strong interannual variability (Vinje, 2001). Minimum sea ice cover is reached in September,
206 only the northeastern shelf areas of Svalbard may experience sea ice during this time of the
207 year. While the southern Yermak Plateau is covered by seasonal sea ice, a thinning of the
208 perennial ice cover above the northern part only takes place in years of exceptionally strong heat
209 supply (National Snow & Ice Data Center, <https://nsidc.org>).

210

211 4. Material and methods

212 The studied Core PS92/039-2 was recovered from the eastern flank of the Yermak Plateau north
213 of Svalbard during RV Polarstern Expedition PS92 in 2015 (Peeken et al., 2016; Fig. 1; Table 1).
214 It provides a continuous sedimentary record, except for the uppermost 15 cm that were disturbed
215 during the recovery process (supplementary Fig. 1). Therefore, a surface sample from the box-
216 corer Core PS92/039-3 (Table 1) was added to the record to have a reference data point
217 representing the modern (Holocene) environment. Line-scan images (performed at the UiT the
218 Arctic University of Norway in Tromsø) were acquired with a Jai CV L107 camera with RGB (red-
219 green-blue) channels at 630 nm, 535 nm and 450 nm, respectively, mounted to an Avaatech
220 XRF core scanner. For environmental magnetic measurements, samples were taken
221 continuously (2.5-3 cm interval) with standard 7cm³ plastic cubes. Low field reversible magnetic
222 susceptibility (k) was measured with an Agico MFK-1-FA Kappabridge (performed at Uppsala
223 University, Sweden). Anhysteretic remanent magnetisation (ARM) was acquired in a peak
224 alternating field of 100 mT with a 50 μ T DC bias field and measured using cryogenic

225 magnetometer (model 2G Enterprise 755R, performed at the University of Bremen, Germany).
226 The susceptibility of ARM (kARM) was calculated from ARM measurements normalised with the
227 50 μ T bias field. Subsequent division with the magnetic susceptibility yields the dimensionless
228 magnetic grain-size sensitive ratio kARM/k (King et al. 1982).

229

230 *Analyses of organic-geochemical bulk parameters*

231 For organic-geochemical analyses, subsamples were taken every 5 cm and stored in glass vials
232 at -20°C. Total organic carbon (TOC) contents were determined using a Carbon-Sulfur Analyser
233 (CS-125, Leco) after decarbonisation of the sediment with hydrochloric acid. The total amounts
234 of carbon (TC) and nitrogen (TN) were determined by means of a Carbon-Nitrogen-Sulfur
235 Analyser (Elementar III, Vario). Assuming that the predominant carbonate phase is calcite,
236 carbonate contents were calculated as $\text{CaCO}_3 = (\text{TC} - \text{TOC}) * 8.333$, where 8.333 is the
237 stoichiometric calculation factor. When using the carbonate data, however, one should consider
238 that a significant proportion of the carbonate at the Yermak Plateau might be dolomite as
239 determined in sediments from nearby Core PS2212-3 (Fig. 1; Vogt, 1997; Vogt et al., 2001). The
240 C/N ratio was calculated using the TOC and TN contents, thereby neglecting the inorganic
241 nitrogen portion (cf., Stein and Macdonald, 2004; supplementary Fig. 2). For organic carbon
242 isotope ($\delta^{13}\text{C}_{\text{org}}$) analysis (performed at the Second Institute of Oceanography, State Oceanic
243 Administration, Hangzhou, China), acidified and homogenised sediment was weighed into a tin
244 foil and wrapped tightly. The determination of $\delta^{13}\text{C}_{\text{org}}$ values was then performed by means of
245 mass spectrometry (Thermo, MAT 253), using Urea Isotopic Working Standard (C-13, N-15) as
246 reference material.

247 *Biomarker analyses*

248 For HBIs and sterol analyses, 5 g of freeze-dried and ground sediment was extracted with an

249 Accelerated Solvent Extractor (DIONEX, ASE 200; 100°C, 5 min, 1,000 psi) using
250 dichloromethane:methanol (2:1 vol/vol) as solvent. Beforehand, the internal standards 7-
251 hexylnonadecane (7-HND; 0.076 µg/sample) and cholesterol-d6 (cholest-5-en-3β-ol-D₆; 10.1
252 µg/sample) were added for biomarker quantification. Hydrocarbons and sterols were separated
253 via open column chromatography using SiO₂ as stationary phase and 5 ml of *n*-hexane followed
254 by 6 ml of ethylacetate:*n*-hexane (2:8 vol/vol) as eluent, respectively. Sterols were silylated with
255 200 µl bis-trimethylsilyl-trifluoroacet-amide (BSTFA; 60°C, 2h) in the next step. Compound
256 identification was carried out with coupled gas chromatography (GC) – mass spectrometry (MS;
257 Agilent 7890B GC - Agilent 5977 A for HBI identification, Agilent 6850 GC - Agilent 5975 C for
258 sterol identification). GC measurements were carried out with the following temperature setup:
259 60°C (3 min), 150°C (heating rate: 15 °C/min), 320°C (heating rate: 10 °C/min), 320°C (15 min
260 isothermal) for the hydrocarbons and 60°C (2 min), 150°C (heating rate: 15 °C/min), 320°C
261 (heating rate: 3 °C/min), 320°C (20 min isothermal) for the sterols. Helium served as carrier gas
262 (1 ml/min constant flow). Specific compound identification was based on the comparison of
263 retention times and mass spectra with literature references (sterols: Boon et al., 1979; Volkman,
264 1986; HBIs: Belt et al., 2007, Brown and Belt, 2016). The concentration of each biomarker was
265 calculated by setting its individual GC-MS ion responses in relation to those of respective
266 internal standards. For the quantification of the sterols (quantified as trimethylsilyl ethers), the
267 molecular ions *m/z* 470 for brassicasterol (as 24-methylcholesta-5,22E-dien-3β-ol), *m/z* 472 for
268 campesterol (as 24-methylcholest-5-en-3β-ol), *m/z* 486 for β-sitosterol (as 24-ethylcholest-5-en-
269 3β-ol) and *m/z* 500 for dinosterol (as 4α,23,24R-trimethyl-5α-cholest-22E-en-3β-ol) were used in
270 relation to the molecular ion *m/z* 464 for the internal standard cholesterol-d₆. For the
271 quantification of IP₂₅ and HBI III, their molecular ions (*m/z* 350 for IP₂₅ and *m/z* 346 for HBI III)
272 were compared to the molecular ion *m/z* 266 for the internal standard 7-HND. The different
273 responses of these ions were balanced by an external calibration curve (see Fahl & Stein,

274 2012). All biomarker concentrations were normalised to the amount of extracted sediment and
275 organic carbon (OC) content.

276 To avoid over- or underestimating the sea ice signal, PIP₂₅ indices were calculated following the
277 equation of Müller et al. (2011): $P_{BIP_{25}} = IP_{25}/(IP_{25}+(\text{brassicasterol} \cdot c))$, where c is a balance
278 factor to compensate significant concentration differences between IP₂₅ and brassicasterol (c =
279 mean IP₂₅ concentration/mean brassicasterol concentrations). Additionally, P_{III}IP₂₅ indices were
280 calculated using HBI III as phytoplankton marker.

281 For GDGT analyses (performed at the Second Institute of Oceanography, State Oceanic
282 Administration, Hangzhou, China), 5 – 10 g of sediment (freeze-dried, ground) was ultrasonically
283 extracted using dichloromethane:methanol (3:1 vol/vol) as solvent. Prior to this step, the internal
284 standard C46 (0.378 µg/sample) was added to the sample. The alcohol fraction containing
285 GDGTs was eluted via open column chromatography using silica gel as stationary phase and
286 dichloromethane:methanol (10 ml; 95:5 vol/vol) as solvent. Compound identification was
287 performed with ultra performance liquid chromatography (Acquity) coupled to atmospheric
288 pressure chemical ionisation mass spectrometry (Xevo TQ MS). The GDGTs were eluted using
289 E1(hexane):E2(hexane:isopropanol) (99:1 vol/vol), with 0.1% isopropanol for 0.5 min (flow rate:
290 0.2 ml/min), then with linear gradient up to 0.5% in 0.6 min (3.5 min isothermal), followed by up
291 to 1% in 1.4 min (2 min isothermal) and finally to 0.1% (4 min isothermal). Single ion recording
292 was set to scan [M+H]⁺ of isoprenoid glycerol dibiphytanyl glycerol tetraethers (OH-GDGT-0,
293 OH-GDGT-1, OH-GDGT-2, i-GDGT-0, i-GDGT-1, i-GDGT-2, i-GDGT-3, Crenarchaeol, Cren';
294 m/z 1318, 1316, 1314, 1302, 1300, 1298, 1296, 1292, 1292, respectively) and [M+H]⁺ of the
295 branched-GDGTs (b-GDGT Ia, b-GDGT IIa, b-GDGT IIIa; m/z 1050, 1036, 1022, respectively).
296 SSTs were calculated using the ring index of OH-GDGTs (supplementary Fig. 3), recommended
297 for polar regions, following the equations presented by Lü et al. (2015): $RI-OH' = ([OH-GDGT-1]$

298 $+ 2*[OH-GDGT-2])/([OH-GDGT-0] + [OH-GDGT-1] + [OH-GDGT-2])$ and $RI-OH' = 0.0382 * SST$
299 $+ 0.1$. All data are available online on PANGAEA.

300

301 5. Results

302 *Lithology and ice rafted debris (IRD)*

303 In the lowermost part of the core (860 - 615 cm), the dominant lithotypes are silty clays
304 intercalated by diamicton layers. An alternation of greyish, dark greyish and brownish coloured
305 intervals can be observed. The overlaying sequence from 615 to 90 cm consists of clayey to silty
306 clayey sediments with a greyish to brownish colour spectrum. Two layers of dark greyish
307 colouration are conspicuous between 310 - 260 cm and 140 - 90 cm. The upper 90 cm are
308 composed of brownish sediments (supplementary Fig. 1). Various bioturbation traces are
309 present throughout the entire record, except for short intervals around 730, 580, 510, 365 and
310 275 cm (supplementary Fig. 1). Peak abundance of IRD (counted on x-radiographs) can be
311 observed in the intervals 650 – 600, 250 – 200 and 145 – 120 cm, while lower amounts of IRD
312 grains are found in 590 – 310 cm core depth (Fig. 2).

313

314 *Organic-geochemical bulk parameters*

315 The TOC content ranges from 0.2 to 1.3 % with slightly enhanced values from 860 to 610 cm as
316 well as distinct maxima from 310 to 250 cm and 140 to 90 cm (Fig. 2). The C/N ratio varies
317 between 4 – 18 in the lowermost part of the core, then changes to slightly lower (~7) and more
318 stable values above 610 cm and lowest values at the surface (~2). Similar to the TOC record,
319 elevated values in the C/N ratio can be observed for the intervals from 310 – 250 cm (up to 12)
320 and 140 – 90 cm (up to 10). The carbonate record shows a highly fluctuating signal around an
321 average of 4 % (Fig. 2). At 415 cm, a sharp rise to a maximum content of 12 % occurs, followed
322 by a sudden drop to mean values at 350 cm core depth. From 70 cm upwards, another sharp

323 increase in the carbonate content occurs with peak values of 13 % at the surface.

324 The $\delta^{13}\text{C}_{\text{org}}$ record is relatively balanced with values ranging between \sim -23 to \sim -25 ‰, except for
325 short-term shifts to lighter values (-27 ‰) at 180 and 640 cm.

326

327 *Biomarkers*

328 The biomarker concentrations vary synchronously and in phase throughout the entire record
329 (Fig. 2). For the lowermost part of the core, highly fluctuating concentrations can be observed
330 with maximum contents of 0.0030 $\mu\text{g/g}$ sediment for IP_{25} , 0.0120 $\mu\text{g/g}$ sediment for HBI III, 0.61
331 $\mu\text{g/g}$ sediment for brassicasterol, 0.15 $\mu\text{g/g}$ sediment for dinosterol and 0.72 $\mu\text{g/g}$ sediment for
332 the terrigenous sterols. At 680 cm core depth, biomarker contents decrease and remain at
333 minimum concentrations to a depth of 390 cm. IP_{25} is mostly absent within this sequence.
334 However, short-term excursions to elevated concentrations occur at 640, 530 and 450 cm (up to
335 0.0014, 0.0025, 0.25, 0.09 and 0.29 $\mu\text{g/g}$ sediment for IP_{25} , HBI III, brassicasterol, dinosterol and
336 the terrigenous sterols, respectively). The sediment sequence between 390 and 90 cm shows a
337 succession of intervals with either minimal to absent and relatively high to maximum biomarker
338 contents (IP_{25} , HBI III, brassicasterol, dinosterol and the terrigenous sterols reach maximum
339 values of 0.0051, 0.0451, 0.72, 0.16 and 1.77 $\mu\text{g/g}$ sediment, respectively). Most prominent
340 peaks occur between 310 - 250 and 150 - 90 cm core depth. These peaks coincide with the
341 most conspicuous excursions to higher values in the TOC and C/N records (Fig. 2). At 90 cm, a
342 drop of all biomarkers to minor concentrations is observed that continues to the uppermost core
343 interval. Between 90 and 40 cm, IP_{25} is completely absent. The surface sample shows enhanced
344 biomarker contents of 0.0071 $\mu\text{g/g}$ sediment for HBI III for IP_{25} , 0.0050 $\mu\text{g/g}$ sediment for HBI III,
345 1.32 $\mu\text{g/g}$ sediment for brassicasterol, 0.07 $\mu\text{g/g}$ sediment for dinosterol and 0.46 $\mu\text{g/g}$ sediment
346 for the terrigenous sterols (Fig. 2). The absolute biomarker concentrations in the surface sample
347 are several orders of magnitude higher than the downcore concentrations. This strong gradient

348 refers to the early biogeochemical degradation of biomarkers in the water column and the upper
349 centimetre of the sediment (Fahl and Stein, 2012; Belt and Müller, 2013).

350

351 6. Discussion

352 6.1 Age model

353

354 The chronostratigraphy of Core PS92/039-2 is based on a combination of AMS¹⁴C dates (Table
355 2) as well as tie points obtained from core correlation and biostratigraphy (Table 3).

356 In the upper part of the core, a significant decrease in the carbonate content and a minimum
357 followed by a maximum in the magnetic susceptibility log are correlated to corresponding trends
358 at Core PS1533-3 (Fig. 1, 3). This core is located in close vicinity to Core PS92/039-2 and has a
359 well-established age model based on radiocarbon dates and $\delta^{18}\text{O}$ stratigraphy for the last 30 ka
360 (Spielhagen et al., 2004). The correlation is further substantiated by similar deflections of the
361 carbonate and magnetic susceptibility records observed in the nearby cores PS2212-3 (Vogt,
362 1997) and PS66/309-1 (Winkelmann et al., 2008a,b). Further downcore, three AMS¹⁴C ages at
363 150, 227.5 and 298 cm allow to pinpoint MIS 2 and 3 in Core PS92/039-2 (Table 2). The distinct
364 minima in magnetic susceptibility and magnetic grain size sensitive kARM/k ratio in Core
365 PS92/039-2 at 320 to 260 cmbsf, based on AMS¹⁴C dating slightly younger than 44.8 ka, can be
366 correlated well to corresponding values of Core PS1533-3 (Fig. 3). Originally, these minima in
367 Core PS1533-3 were dated to MIS 4 (Spielhagen et al., 2004), but our new data suggest a MIS 3
368 age. Further investigation is needed to clarify these discrepancies, this study, however, relies on
369 the AMS¹⁴C ages. The occurrence of the biostratigraphic marker *Pullenia bulloides* at 388 cm
370 (Peeken et al., 2016) is considered to indicate MIS event 5.1 (~81 ka, Haake and Pflaumann,
371 1989), as in the cores PS2212-3, PS2122 and PS2123 (Vogt, 1997; Vogt et al., 2001). The MIS
372 5/6 boundary is well-defined in nearby Core PS1533-3, based on ¹⁰Be- and $\delta^{18}\text{O}$ -stratigraphy

373 (Nowaczyk et al., 1994; Spielhagen et al., 2004). A decrease of the magnetic susceptibility at
374 this transition is also recorded for the cores PS2212-3 (Nowaczyk et al., 1994) and PS66/309-1
375 (Winkelmann et al., 2008b) and for Core PS92/039-2, ensuring a clear allocation of this stage
376 boundary to 610 cm core depth. According to linear extrapolation, the core base is of early MIS 6
377 age (~180 ka; Fig. 4). This estimation is, however, unrealistic given the fact that the
378 sedimentation rates of MIS 6 most likely differ from those of MIS 5. Previous studies north of
379 Spitsbergen described significantly higher sedimentation rates in MIS 6 compared to the
380 following MIS 5 interval (Knies et al., 2001; Stein et al., 2001; Winkelmann et al., 2008a). In the
381 neighbouring Core PS66/309-1, the sedimentation rates of MIS 6 exceed those of MIS 5 by a
382 factor of ~2 (Winkelmann et al., 2008a). Assuming similar changes for Core PS92/039-2, the
383 more probable age of the core base is ~160 ka (Fig.4).

384 An additional, independent confirmation of this age model is given by the mineral magnetic data,
385 i.e., the kARM/k ratio representing a magnetic mineral grain size proxy. Previous studies have
386 described a noticeable similarity between the kARM/k ratio and $\delta^{18}\text{O}$ data (Nowaczyk et al.,
387 1994; O'Regan et al., 2008; Xuan et al., 2012). Thus, the correlation of this ratio at Core
388 PS92/039-2 to the global benthic $\delta^{18}\text{O}$ record of Lisiecki and Raymo (2005) seems to support
389 our proposed age model and allows a tentative definition of the substages MIS 5a, 5c and 5e
390 (Fig. 3). However, one should keep in mind that the relation between these parameters is not
391 fully understood so far and that other factors, such as post-depositional diagenesis, might have
392 an impact on magnetic grain size fluctuations (Xuan et al., 2012).

393

394 5.2 Organic carbon accumulation at the Yermak Plateau related to sea ice – ice sheet coupling

395

396 Distinct layers rich in terrigenous OC have been traced in cores along the northern Eurasian
397 margin of the Arctic Ocean during the late Quaternary (e.g., Elverhøi et al., 1995; Knies and

398 Stein, 1998; Stein et al., 2001; Vogt et al., 2001; Birgel and Stein, 2004; Winkelmann et al.,
399 2008a). Coinciding with episodes of intense glaciation on Svalbard, these intervals were linked
400 to movements of the SBIS. Probable source areas for the terrigenous organic matter are the
401 outcropping OC-rich Mesozoic bedrocks in the northern Barents Sea and on the
402 Spitsbergenbanken (Elverhøi et al., 1989, 1995).

403 Winkelmann et al. (2008a) investigated this phenomenon in more detail on a series of cores
404 reflecting the paleoceanographic situation of the Sophia Basin north of Svalbard over the last
405 200 ka. At least five sediment layers possessing similar mineralogical, sedimentological and
406 organic-geochemical features could be correlated and were termed “Terrigenous Input Events”
407 (TIEs). The most striking features of these intervals are enhanced OC contents, elevated C/N
408 ratios, lowest to zero carbonate contents and coarser grain sizes. The chronology of the TIEs
409 was assigned to the onset of the late Saalian glaciation (TIE 4), Termination II (TIE 3), the onset
410 and termination of the Mid Weichselian glaciation (TIE 2), the LGM (TIE 1) and Termination I
411 (TIE 0). No increased terrigenous input has been observed in connection with the supposed
412 glaciation around 110 ka (Mangerud et al., 1998), suggesting that this phase of ice sheet
413 formation was probably more pronounced at the western continental margin of Svalbard
414 (Winkelmann et al., 2008a).

415 In Core PS92/039-2 from the eastern Yermak Plateau, three comparable sediment horizons can
416 be identified for the last 160 ka (Fig. 6). According to the high concentration of OC, these
417 horizons are visually conspicuous because of their dark greyish colour (Fig. 2). The
418 predominance of terrigenous OC is indicated by elevated C/N ratios and a tendency to lighter
419 $\delta^{13}\text{C}_{\text{org}}$ values. Meanwhile, the carbonate content is significantly lowered. In addition to these
420 features that were thoroughly described by previous studies, our biomarker data complete the
421 overall picture of these events with regard to sea ice conditions at that time. All intervals are
422 characterised by peak accumulation rates of the sea ice proxy IP_{25} synchronously with maximum

423 fluxes of the marine biomarkers brassicasterol, dinosterol and HBI III and the landplant-derived
424 sterols campesterol and β -sitosterol (Fig. 2). Hence, conditions must have been favourable for
425 both sea ice and open water algal growth accompanied by a continuous input of terrigenous
426 material. These processes were previously reported as typical features along the ice edge
427 (Smith, 1987, Stein et al., 2016). Terrigenous material is entrapped during the formation of new
428 sea ice in the Kara and Laptev Sea shelf regions, transported via the Transpolar Drift and
429 released at the ice edge due to ablative processes (Reimnitz et al., 1994; Stein et al., 1994). The
430 resulting high-nutrient suspension in the surface water facilitates primary productivity (Sakshaug,
431 2004). As carbonate dissolution is often enhanced in areas of high productivity and seasonal sea
432 ice formation, this might explain the low carbonate content during these events (Knies, 1994;
433 Steinsund and Hald, 1994). For sea ice diatoms living in/at the underside of the ice, the
434 environmental setting along the ice edge is most favourable due to light and nutrient availability
435 (Fahl and Stein, 2012). Such marginal sea ice conditions are indicated by $P_{BIP_{25}}$ indices
436 between 0.5 and 0.75 (Fig. 5). The simultaneous input of marine and terrestrial organic matter is
437 further reflected in the $\delta^{13}C_{org}$ signature of these specific layers. Although the predominance of
438 terrigenous organic matter is expressed by a shift towards lighter values, typical terrigenous
439 endmember values around -27 ‰ (Fernandes and Sicre, 2000) are not reached. Obviously, the
440 concurrent admixture of isotopically enriched phytoplankton (-20 ‰; Knies et al., 2003) and ice
441 algae (-15 to -8 ‰; Gibson et al., 1999) alters the $\delta^{13}C_{org}$ signal.

442 The chronology of the OC events at the Yermak Plateau (PS92/039-2) seems to be connected to
443 major deglaciation intervals on Svalbard (Fig. 6; cf., Winkelmann et al., 2008a). As the SBIS
444 started to retreat after its maximal extensions around 140, 60 and 20 ka, enormous discharges
445 of glacially eroded material took place. Captured by meltwater plumes and dense bottom
446 currents, the reworked material spread along the northern continental margins (Knies and Stein,
447 1998). The lateral advection of the fine material to the core site significantly supported the

448 preservation of organic matter released at the nearby ice margin. Knies and Stein (1998) found
449 highest sedimentary contents of marine organic matter in the northern Barents Sea as a result of
450 scavenging on reworked terrigenous particles (“mineral ballast effect”). The formation of
451 aggregates enables an efficient vertical transport through the water column and a subsequent
452 burial at the sea floor (Ittekkot et al., 1992; Knies and Stein, 1998). A more detailed evaluation of
453 the individual events with regard to the predominant paleoceanographic situation is given in the
454 following chapter.

455

456 5.3 Sea ice variations at the eastern Yermak Plateau over the last 160 ka

457 *The Saalian (MIS 6; 160 – 130 ka)*

458

459 Reconstructions of the QUEEN (Quaternary Environment of the Eurasian North) programme
460 revealed that the Saalian glacial was the most extensive glaciation in northern Eurasia during the
461 late Quaternary (Svendsen et al., 2004). Ice sheets covered the Barents and Kara Seas to the
462 shelf edge and probably the Severnaya Zemlya Archipelago (Polyak et al., 2001; Astakhov,
463 2004; Jakobsson et al., 2016). On the shelves north of Svalbard, some areas show streamlined
464 patterns on the sea floor in water depths of up to 800 m with a proposed age of the MIS 6
465 glaciation (e.g., Vogt et al., 1994; Dowdeswell et al., 2010; Jakobsson et al., 2010). Possible
466 explanations for the observed features include the northward expansion of the SBIS onto the
467 Yermak Plateau, the grounding of large fragments of glacial ice, an armada of deep icebergs
468 and the existence of a pan-Arctic ice shelf (Svendsen et al., 2004; Dowdeswell et al., 2010;
469 Jakobsson et al., 2016).

470 Based on our biomarker records of Core PS92/039-2, there is no indication for an ice sheet
471 covering the northern Yermak Plateau throughout the entire MIS 6. The sea ice proxy IP₂₅
472 fluctuates around mean values of 0.001 $\mu\text{g/g}$ sediment intercalated by short intervals of near

473 zero contents (Fig. 6). Nonetheless, a more or less continuous input can be observed during this
474 interval, indicating seasonally open-water conditions. Simultaneously with enhanced IP_{25} fluxes,
475 increased accumulation of the phytoplankton (brassicasterol, dinosterol, HBI III) and terrigenous
476 (campesterol, β -sitosterol) biomarkers can be observed during most parts of MIS 6, suggesting
477 the presence of marginal sea ice cover at the Yermak Plateau at that time. A combination of
478 katabatic winds from the protruded SBIS and upwelling of relatively warm AW along its shelf
479 break might have triggered the formation of a coastal polynya along the northern Barents Sea
480 margin (cf., Knies et al., 1999; 2000; Stein et al., 2017b) with the parallel formation of a
481 stationary ice margin at the eastern Yermak Plateau (Fig. 8). A similar MIS 6 scenario is
482 described for the East Siberian continental margin, where the northward extension of the East
483 Siberian Chukchi Ice Sheet (Niessen et al., 2013) probably triggered the formation of a polynya
484 in front of it, enabling ice diatom and phytoplankton production at the southern Lomonosov Ridge
485 (Stein et al., 2017b). Relatively high OC contents of predominantly terrigenous origin (low $\delta^{13}C$
486 values, high C/N ratios) indicate the input of glacially eroded material along the Eurasian
487 continental margin at that time (Knies et al., 2000, 2001). The distinct variability of the biomarker
488 and the organic-geochemical bulk parameter records may indicate rather unstable
489 oceanographic conditions. The stratification of MIS 6 sediments in Core PS92/039-2 further
490 implies several alterations of the environmental and sedimentary regime (Fig. 2). This means
491 that the sea ice margin may have shifted back and forth several times during MIS 6, probably
492 linked to the glaciation mode of Svalbard. An unstable behaviour of the SBIS, with repeated
493 waxing and waning to the outer shelf, is reported for late MIS 6 as a result of episodically
494 intensified advection of warm AW (Knies et al., 2001; Matthiessen et al., 2001). Similar
495 occasional destabilisation of the ice sheet might have occurred in the course of strengthened
496 AW inflow around 145, 165 and 180 ka (Lloyd et al., 1996; Hebbeln and Wefer, 1997;
497 Wollenburg et al., 2001).

498 A drop to zero fluxes of IP_{25} and minimum fluxes of the phytoplankton markers as well as related
499 $P_{BIP_{25}}$ and $P_{IIIIP_{25}}$ maxima towards the end of MIS 6 indicates the establishment of more severe
500 ice cover at the Yermak Plateau (Fig. 7). The sea ice margin possibly followed the southward
501 migration of the SBIS as the coastal polynya in front of the ice sheet formed back. Now covering
502 the Yermak Plateau with perennial sea ice, any primary production or material release is
503 prohibited (Fig. 8). An alternative explanation might be a short expansion of the SBIS onto the
504 Yermak Plateau. However, the biomarker data allow no differentiation between a perennial sea
505 ice cover and a km-thick ice shelf.

506 The collapse of major parts of the SBIS after the Penultimate Glacial Maximum around 140 ka
507 (Colleoni et al., 2016) was linked to increasing insolation coupled to strengthened inflow of AW
508 along the western Svalbard Archipelago (Spielhagen et al., 2004). In Core PS92/039-2, peak
509 contents of terrigenous OC (C/N ratio ~15) accompanied by slightly enhanced biomarker
510 abundances may indicate the influence of the distinct meltwater event reconstructed by previous
511 studies around Termination II (Knies et al., 2001; Knies and Vogt, 2003; Spielhagen et al.,
512 2004). Winkelmann et al. (2008a) described increased OC accumulation at times of “Terrigenous
513 Input Event 3”. Fed by the thawing ice sheet, such meltwater plumes flow downslope and
514 incorporate fine-grained, mainly terrigenous sediment on the way (cf., Birgel and Hass, 2004).
515 By absorption onto these suspended particles, marine organic matter produced in the nearby
516 MIZ may have been transported to areas covered by perennial sea ice, hence, the Yermak
517 Plateau during that time (Soltwedel et al., 2000; Rutgers van der Loeff et al., 2002).

518

519 *The Eemian and the early Weichselian (MIS 5; 130 – 71 ka)*

520

521 During MIS 5, biomarker concentrations are variable, but among their lowest values in the entire
522 record (Fig. 6). The resulting $P_{BIP_{25}}$ and $P_{IIIIP_{25}}$ indices indicate most severe ice conditions with

523 perennial sea ice cover (Fig. 7). The presence of sea ice is further indicated by (summer) SSTs
524 below 2.5 °C (Fig. 6; cf., Sarnthein et al., 2003). The IRD signal is strongly diminished,
525 additionally suggesting a closed ice cover. In contrast to that, previous studies described MIS 5
526 as a period characterised by SSTs comparable to the recent or even warmer ones (e.g.,
527 Matthiessen and Knies, 2001; Matthiessen et al., 2001; Spielhagen et al., 2004, Bauch, 2013).
528 Along the Barents Sea continental margin, the presence of sea ice was significantly reduced,
529 especially during the interstadials MIS 5e, 5c and 5a (Wollenburg et al., 2001; Chauhan et al.,
530 2014; Stein et al., 2017b). However, these observations mainly derive from cores situated
531 directly within the inflow path of AW to the Arctic Ocean. Upwelling of this relatively warm water
532 mass might have triggered the formation of open water areas on the shelves west and north of
533 Svalbard, especially in combination with the insolation maxima around 125, 100 and 80 ka
534 (Laskar et al., 2004). Nonetheless, the more interior parts of the Arctic Ocean remained
535 unaffected (or affected to a lesser degree) by the inflow of warm AW and experienced
536 predominantly permanent ice conditions (Stein et al., 2017b) with the summer sea ice boundary
537 positioned slightly southward of the core position of PS92/039-2 on the eastern Yermak Plateau.
538 However, the abundance of various ichnofossils throughout MIS 5 might indicate occasional
539 nutrient transfer to the seafloor caused by ephemeral break-up of the sea ice cover
540 (supplementary Fig. 1).

541 Two phases of moderately enhanced IP_{25} and phytoplankton marker fluxes and resulting
542 lowered $P_{BI}IP_{25}$ and $P_{III}IP_{25}$ indices around 112 and 95 ka indicate phases of reduced sea ice
543 cover. This is further supported by slightly enhanced input of the terrigenous sterols implying a
544 release of material trapped in sea ice due to melting processes. The intervals coincide with
545 distinct insolation minima and might represent the colder substages 5d and 5b (Fig 6; cf., Laskar
546 et al., 2004). Terrestrial mapping and OSL (optically stimulated luminescence) dating of tills
547 suggest the presence of huge ice sheets covering northern Siberia and the Kara Sea to the shelf

548 edge during the early Weichselian glaciation (MIS 5d-b; Svendsen et al., 2004), coinciding with
549 an extended sea ice cover at the northern Barents Sea continental margin (Stein et al., 2017b).
550 Observations from the western continental margin of Svalbard indicate a major ice sheet
551 advance during substage 5d followed by a less pronounced, more local one during 5b
552 (Mangerud et al., 1996, 1998). In any case, no indication for a major glaciation of the shelf
553 regions northeast of Svalbard could be identified during this period (Knies et al., 1999, 2000,
554 2001; Winkelmann et al., 2008a). In Core PS92/039-2, the almost constant records of the OC
555 content and the C/N ratio clearly indicate a reduced input of glacially reworked material from the
556 Svalbard region. However, minor northward advances of the SBIS might have triggered
557 ephemeral break-up of the permanent ice cover above the Yermak Plateau, permitting some ice
558 diatom and phytoplankton production. These intervals of seasonally open water are further
559 recorded by moderate IRD input. However, the age control within MIS 5 needs to be improved in
560 order to interpret the paleoceanographic situation in more detail.

561

562 *The middle Weichselian (MIS 4 and 3; 71 – 29 ka)*

563

564 An interval of enhanced AW inflow is recorded in cores along the northern Barents Sea
565 continental margin for late MIS 5 and early MIS 4 (e.g., Matthiessen and Knies, 2001;
566 Wollenburg et al., 2001; Chauhan et al., 2014). It is suggested that the resulting open-water
567 areas in the Nordic Seas and parts of the Arctic Ocean acted as essential moisture sources for
568 the subsequent ice sheet growth initiated by declining insolation (minimum around 72 ka; Laskar
569 et al., 2004). Spielhagen et al. (2004) even claimed an “optimum combination” of AW intrusion
570 (moisture supply) and climatic conditions (temperature and pressure gradients) for MIS 4,
571 leading to fast glaciation of northern Eurasia. First evidence for an ice sheet advance on
572 Svalbard is reflected in the IRD records from Core PS2138-1 between 75 and 70 ka (Knies et al.,

573 2000, 2001). Coevally, ice diatom and phytoplankton production increased at the Yermak
574 Plateau, indicated by rising sedimentary abundances of IP₂₅, brassicasterol and HBI III in Core
575 PS92/039-2. Higher fluxes likely occurred as a result of reduced ice thickness, hence better light
576 penetration and nutrient availability. As these enhanced abundances are also reflected in the
577 content of the terrigenous biomarkers, the establishment of a stationary sea ice margin above
578 the Yermak Plateau seems to accompany the MIS 5/4 transition. This is also in accordance with
579 a decrease in the P_BIP₂₅ and P_{III}IP₂₅ indices indicating less severe and probably marginal sea ice
580 cover. Similar to MIS 6, the formation of a coastal polynya in front of the protruding ice sheet
581 might have led to a northward shift of the sea ice margin. However, no enhanced input of
582 glacially eroded material from Svalbard is evident in Core PS92/039-2 at that time (TOC ~0.6 %,
583 C/N ratio ~8; Fig. 6). As already suggested by other studies from the region, a more restricted
584 ice sheet expansion during MIS 4 is likely. The greater distance of the ice shelf edge is also
585 indicated by lower bulk accumulation rates compared to the glacial MIS 6 and 2 (Fig. 6; Knies et
586 al., 2000). Hence, the intensive intrusion of AW in early MIS 4 might have been more decisive for
587 the formation of wide ice-free areas north of Svalbard than the extent of the SBIS. As the inflow
588 weakens, the sea ice cover rapidly thickens, marked by a sudden drop of biomarker
589 concentrations around 67 ka. Near zero biomarker and OC fluxes highlight the presence of a
590 permanent ice cover at the Yermak Plateau until 50 ka, inhibiting primary production and the
591 release of terrigenous material.

592 Exceptionally high accumulation rates of the sea ice proxy IP₂₅, OC and marine and terrigenous
593 sterols reveal an enormous material discharge between 50 and 42 ka. A distinct rise in the C/N
594 ratio highlights the predominantly terrigenous origin of the organic matter.

595 Previous studies associated early MIS 3 with a series of meltwater events (Mangerud et al.,
596 1998; Knies et al., 2000; Chauhan et al., 2014), probably steered by the northward breakthrough
597 of huge meltwater lakes in the Siberian hinterland (Spielhagen et al., 2004). Fine-grained

598 sediments were flushed off the shelf areas of the Kara and Barents Seas by huge meltwater
599 plumes and laterally advected to the core site at the Yermak slope. The resulting high
600 sedimentary fluxes probably promoted the burial and preservation of material released at the
601 nearby ice margin (Knies and Stein, 1998). Creating a stratified water column with a thick
602 freshwater layer on the surface, this outburst would have encouraged the formation of new sea
603 ice and, in turn, delayed the deglaciation due to a significant cooling of the ocean triggered by
604 positive ice albedo feedback mechanisms (Ruddiman and McIntyre, 1981). Indeed, late MIS 3 is
605 characterised by more severe ice conditions above the Yermak Plateau, indicated by $P_{BIP_{25}}$
606 indices mostly between 0.7 and 1 (Fig. 7). The general close proximity to the sea ice margin
607 seems to be supported by SSTs between -2.5 and 2.5°C (Fig 6; cf., Sarnthein et al., 2003). Two
608 sequences of slightly enhanced fluxes of OC as well as sea ice, phytoplankton and terrigenous
609 biomarkers can be observed around 38 and 33 ka (Fig. 6). Significantly smaller in amplitude
610 than the event observed around 45 ka, these might reflect a more local influence of the ongoing
611 deglaciation of the Eurasian hinterlands during MIS 3. The continuous input of glacially eroded
612 material along the western continental margin of Svalbard points to a maintenance of minor
613 glaciations on Svalbard prior to the renewed ice sheet growth during latest MIS 3 (Spielhagen,
614 1991). The trigger for the episodic ice sheet disintegration might be associated with intervals of
615 enhanced inflow of relatively warm AW during MIS 3 (Dokken and Hald, 1996; Hald et al., 2001).
616 These so-called “Nordway Events” (Hebbeln and Wefer, 1997) are characterised by increased
617 biological productivity and thus open water conditions in parts of the Nordic Seas and the Fram
618 Strait (Hebbeln et al., 1994; Dokken and Hald, 1996; Rasmussen and Thomsen, 2008). The
619 enhanced sedimentary biomarker abundances in Core PS92/039-2 that might be correlated with
620 these events, imply a close proximity to the highly productive MIZ throughout MIS 3. The
621 material discharge associated with the ice sheet decay on Svalbard probably fostered the burial
622 and preservation of the organic matter produced at the nearby ice edge.

623

624 *The late Weichselian and Holocene (MIS 2 and 1; 29 – 0 ka)*

625

626 The variability of sea ice cover at the western Yermak Plateau (i.e., Core PS2837-5; Fig. 1) was
627 studied in detail by Müller et al. (2009) for the last 30 ka. Due to a comparably low sample
628 resolution for this time interval in Core PS92/039-2, only a rough comparison of the two core
629 sites with regard to sea ice conditions is possible.

630 For most of the time interval between 30 and 20 ka, near zero contents of IP₂₅ and brassicasterol
631 suggest the presence of perennial sea ice at the western Yermak Plateau. This is followed by a
632 gradual rise of IP₂₅ and brassicasterol indicating improved conditions for ice diatom and
633 phytoplankton growth. The resulting P_BIP₂₅ index reveals the prevalence of seasonal sea ice that
634 continues through the Holocene (Fig. 7; Müller et al., 2009).

635 The eastern Yermak Plateau (i.e., Core PS92/039-2), on the other hand, experienced extended
636 sea ice around 30 ka, followed by an interval predominated by marginal sea ice (Fig. 7). Similar
637 to the glaciations during MIS 6 and 4, katabatic winds from the protruding ice sheet and/or
638 strengthened AW intrusion probably led to the formation of a coastal polynya north of Svalbard
639 (Fig. 8). After reaching minimum insolation during the Last Glacial Maximum ~20 ka, the SBIS
640 became more unstable (Knies et al., 2000; Chauhan et al., 2014). Rapid disintegration started
641 around ~15 ka with the onset of the Bølling warm period (Ruddiman and McIntyre, 1981;
642 Fairbanks, 1989; Rasmussen et al., 2002). Coincidentally, peak accumulation rates of terrigenous
643 OC, IP₂₅ and the phytoplankton markers in Core PS92/039-2 indicate huge material discharge
644 associated with the deglaciation process (Fig. 6). Winkelmann et al. (2008a) described the
645 enhanced lithogenic flux observed in cores along the northern Barents Sea continental margin at
646 that time as “Terrigenous Input Event 0”. The final retreat of the ice sheet to the coastline of
647 Svalbard around 13 ka (Landvik et al., 1998; Mangerud et al., 1998; Hughes et al., 2016)

648 apparently resulted in the re-establishment of perennial sea ice at the eastern Yermak Plateau,
649 indicated by a sudden drop of biomarker contents in Core PS92/039-2. Like the western Yermak
650 Plateau, the eastern part experienced seasonal sea ice during the late Holocene, indicated by
651 enhanced biomarker fluxes in Core PS92/039-2 (Fig. 6).

652 Taken together, the sea ice conditions at both core sites follow a comparable trend with a few
653 discrepancies probably indicating the local environmental forces. Hence, the eastern Yermak
654 Plateau seems to be more strongly influenced by the northward expansion of the SBIS while the
655 western part is likely more impacted by AW that flows along its western flank.

656

657 6. Conclusions

658

659 Our biomarker-based reconstruction of sea ice conditions at the eastern Yermak Plateau during
660 the last 160 ka reveals novel information about the complex interplay between sea ice and
661 different environmental forces that decisively affect the sedimentation regime throughout glacial-
662 interglacial cycles. Our study suggests that a simplified scenario with more sea ice during
663 glacials and less sea ice during interglacials is not constantly applicable for the study area.

664 The following statements can be made:

- 665 · During glacial intervals, the eastern Yermak Plateau experienced periodically marginal sea ice
666 conditions. The combination of katabatic winds from the protruding SBIS in combination
667 with upwelling of warm Atlantic Water along its shelf edge probably led to the formation of
668 a coastal polynya north of Svalbard with contemporaneous sea ice margin occurrence in
669 the vicinity of the site of Core PS92/039-2.
- 670 · An advance of the SBIS onto the Yermak Plateau throughout the (entire) Saalian glaciation
671 can not be supported by our new biomarker data. However, the environment north of
672 Svalbard appeared to be a highly dynamic system during MIS 6 with repeated waxing

673 and waning of the SBIS to the outer shelf and possibly temporary onto the Yermak
674 Plateau.

- 675 · Severe, but variable sea ice cover prevailed at the Yermak Plateau during interglacial periods.
- 676 · Maximum fluxes of OC, IP₂₅ and the phytoplankton and terrigenous biomarkers can be
677 observed during deglaciation phases, when meltwater plumes from the disintegrating ice
678 sheets in northern Eurasia spread high amounts of glacially reworked material along the
679 continental margins.
- 680 · The comparison of the sea ice variability between the eastern and the western Yermak
681 Plateau over the last 30 ka highlights the regional impact of different environmental
682 forces like ice sheet extent and Atlantic Water inflow.

683 Acknowledgements

684 We thank the captain and the crew of R/V Polarstern for excellent cooperation during the
685 TRANSSIZ cruise PS92 (grant-no. AWI_PS92_00) in 2015. Thanks to W. Luttmer for technical
686 support during the laboratory work and to Ingrid L. Olsen and Sigrun Hegstad for supporting the
687 acquisition of the line-scan images. Thanks to Simon Belt and colleagues (Biogeochemistry
688 Research Centre, University of Plymouth) for providing the internal standard for the IP₂₅
689 analyses. The paper is a contribution to the German-Chinese project with the title “Natural
690 variability of Arctic sea ice and its significance for global climate change and OC cycle”.
691 Financial support was given by the Federal Ministry of Education and Research (BMBF, project-
692 no. 01DO14004), the National Natural Science Foundation of China (project-no. 41406217) and
693 by the Swedish Research Council (grant no. 2014-4108). The authors would like to thank the
694 editor and two anonymous reviewers for their thorough and helpful comments to improve the
695 manuscript.

696

697 References

698

699 Aagaard, K., 1982. Inflow from the Atlantic Ocean to the Polar Basin. In: Rey, L. (Eds.), The

700 Arctic Ocean. Comité Arctique International, Monaco, pp. 69-82.

701 Aagaard, K., Foldvik, A., Hillman, S.R., 1987. The West Spitsbergen Current - Disposition and
702 Water Mass Transformation. *Journal of Geophysical Research: Oceans* 92, 3778-3784.

703 Aagaard, K., Coachman, L., 1968. The East Greenland Current north of Denmark Strait: Part II.
704 *Arctic* 21, 181-200.

705 Astakhov, V., 2004. Middle Pleistocene glaciations of the Russian north. *Quaternary Science*
706 *Reviews* 23, 1285-1311.

707 Bauch, H.A., 2013. Interglacial climates and the Atlantic meridional overturning circulation: Is
708 there an Arctic controversy? *Quaternary Science Reviews* 63, 1-22.

709 Belt, S.T., Allard, W.G., Massé, G., Robert, J.M., Rowland, S.J., 2000. Highly branched
710 isoprenoids (HBIs): Identification of the most common and abundant sedimentary
711 isomers. *Geochimica et Cosmochimica Acta* 64, 3839-3851.

712 Belt, S.T., Massé, G., Rowland, S.J., Poulin, M., Michel, C., LeBlanc, B., 2007. A novel chemical
713 fossil of palaeo sea ice: IP₂₅. *Organic Geochemistry* 38, 16-27.

714 Belt, S.T., Massé, G., Vare, L.L., Rowland, S.J., Poulin, M., Sicre, M.-A., Sampei, M., Fortier, L.,
715 2008. Distinctive ¹³C isotopic signature distinguishes a novel sea ice biomarker in Arctic
716 sediments and sediment traps. *Marine Chemistry* 112, 158-167.

717 Belt, S.T., Cabedo-Sanz, P., Smik, L., Navarro-Rodriguez, A., Berben, S.M.P., Knies, J., Husum,
718 K., 2015. Identification of paleo Arctic winter sea ice limits and the marginal ice zone:
719 Optimised biomarker-based reconstructions of late Quaternary Arctic sea ice. *Earth and*
720 *Planetary Science Letters* 431, 127-139.

721 Belt, S.T., Müller, J., 2013. The Arctic sea ice biomarker IP₂₅: a review of current understanding,
722 recommendations for future research and applications in palaeo sea ice reconstructions.
723 *Quaternary Science Reviews* 79, 9-25.

724 Berben, S.M.P., Husum, K., Navarro-Rodriguez, A., Belt, S.T., Aagaard-Sørensen, S., 2017.
725 Semi-quantitative reconstruction of early to late Holocene spring and summer sea ice
726 conditions in the northern Barents Sea. *Journal of Quaternary Science* 32, 587-603.

727 Birgel, D., Hass, H.C., 2004. Oceanic and atmospheric variations during the last deglaciation in
728 the Fram Strait (Arctic Ocean): a coupled high-resolution organic-geochemical and
729 sedimentological study. *Quaternary Science Reviews* 23, 29-47.

730 Birgel, D., Stein, R., 2004. Northern Fram Strait and Yermak Plateau: distribution, variability and
731 burial of organic carbon and paleoenvironmental implications. In: Stein, R., Macdonald,

732 R.W. (Eds.), *The Organic Carbon Cycle in the Arctic Ocean*, Springer-Verlag, Berlin, pp.,
733 279-294.

734 Boon, J.J., Rijpstra, W.I.C., Delange, F., Deleeuw, J.W., Yoshioka, M., Shimizu, Y., 1979. Black
735 Sea Sterol - Molecular Fossil for Dinoflagellate Blooms. *Nature* 277, 125-127.

736 Bordowskiy, O.K., 1965. Sources of organic matter in marine basins. *Marine Geology* 3, 5–31.

737 Bourke, R., Weigel, A., Paquette, R., 1988. The westward turning branch of the West
738 Spitsbergen Current. *Journal of Geophysical Research: Oceans* 93, 14065-14077.

739 Brassell, S.C., Eglinton, G., Marlowe, I.T., Pflaumann, U., Sarntheim, M., 1986. Molecular
740 stratigraphy: a new tool for climate assessment. *Nature* 320, 129-133.

741 Broecker, W.S., 1997. Thermohaline circulation, the Achilles heel of our climate system: Will
742 man-made CO₂ upset the current balance? *Science* 278, 1582-1588.

743 Brown, T., Belt, S., Tatarek, A., Mundy, C., 2014. Source identification of the Arctic sea ice proxy
744 IP₂₅. *Nature communications* 5, 4197.

745 Brown, T.A., Belt, S.T., 2016. Novel tri- and tetra-unsaturated highly branched isoprenoid (HBI)
746 alkenes from the marine diatom *Pleurosigma intermedium*. *Organic Geochemistry* 91,
747 120-122.

748 Chauhan, T., Rasmussen, T.L., Noormets, R., Jakobsson, M., Hogan, K.A., 2014. Glacial history
749 and paleoceanography of the southern Yermak Plateau since 132 ka BP. *Quaternary*
750 *Science Reviews* 92, 155-169.

751 Clark, P.U., Dyke, A.S., Shakun, J.D., Carlson, A.E., Clark, J., Wohlfarth, B., Mitrovica, J.X.,
752 Hostetler, S.W., McCabe, A.M., 2009. The Last Glacial Maximum. *Science* 325, 710-714.

753 Coachman L.K., Aagaard K., 1974. *Physical Oceanography of Arctic and Subarctic Seas*. In:
754 Herman Y. (Eds.), *Marine Geology and Oceanography of the Arctic Seas*. Springer,
755 Berlin, Heidelberg, pp. 1-72.

756 Colleoni, F., Wekerle, C., Naslund, J.O., Brandefelt, J., Masina, S., 2016. Constraint on the
757 penultimate glacial maximum Northern Hemisphere ice topography (approximate to 140
758 kysr BP). *Quaternary Science Reviews* 137, 97-112.

759 Comiso, J.C., Parkinson, C.L., Gersten, R., Stock, L., 2008. Accelerated decline in the Arctic sea
760 ice cover. *Geophysical Research Letters* 35, L01703.

761 Dieckmann, G.S., Hellmer, H.H., 2008. The Importance of Sea Ice: An Overview. In: Thomas,
762 D.N., Diekmann, G.S. (Eds.), *Sea Ice: an introduction to its physics, chemistry, biology,*
763 *and geology*. Blackwell Science, Oxford, pp. 1-21.

764 Dokken, T.M., Hald, M., 1996. Rapid climatic shifts during isotope stages 2-4 in the Polar North
765 Atlantic. *Geology* 24, 599-602.

766 Dowdeswell, J.A., Jakobsson, M., Hogan, K.A., O'Regan, M., Backman, J., Evans, J., Hell, B.,
767 Löwemark, L., Marcussen, C., Noormets, R., Cofaigh, C.O., Sellen, E., Solvsten, M.,
768 2010. High-resolution geophysical observations of the Yermak Plateau and northern
769 Svalbard margin: implications for ice-sheet grounding and deep-keeled icebergs.
770 *Quaternary Science Reviews* 29, 3518-3531.

771 Eglinton, T.I., Eglinton, G., 2008. Molecular proxies for paleoclimatology. *Earth and Planetary*
772 *Science Letters* 275, 1-16.

773 Elverhøi, A., Pfirman, S.L., Solheim, A., Larssen, B.B., 1989. Glaciomarine Sedimentation in
774 Epicontinental Seas Exemplified by the Northern Barents Sea. *Marine Geology* 85, 225-
775 250.

776 Elverhøi, A., Svendsen, J.I., Solheim, A., Andersen, E.S., Milliman, J., Mangerud, J., Hooke,
777 R.L., 1995. Late Quaternary sediment yield from the high Arctic Svalbard area. *The*
778 *Journal of Geology* 103, 1-17.

779 Fahl, K., Stein, R., Gaye-Haake, B., Gebhardt, C., Kodina, L.A., Unger, D., Ittekkot, V., 2003.
780 Biomarkers in surface sediments from the Ob and Yenisei estuaries and southern Kara
781 Sea: Evidence for particulate organic carbon sources, pathways, and degradation. In:
782 Stein, R., Fahl, K., Fütterer, D.K., Galimov, E.M., Stepanets, O.V. (Eds). *Siberian river*
783 *run-off in the Kara Sea: characterisation, quantification, variability, and environmental*
784 *significance. Proceedings in Marine Sciences vol 6. Elsevier, Amsterdam, pp 329–348.*

785 Fahl, K., Stein, R., 2007. Biomarker records, organic carbon accumulation, and river discharge in
786 the Holocene southern Kara Sea (Arctic Ocean). *Geo-Marine Letters* 27, 13–25.

787 Fahl, K., Stein, R., 2012. Modern seasonal variability and deglacial/Holocene change of central
788 Arctic Ocean sea-ice cover: New insights from biomarker proxy records. *Earth and*
789 *Planetary Science Letters* 351, 123-133.

790 Fairbanks, R.G., 1989. A 17,000-Year Glacio-Eustatic Sea-Level Record - Influence of Glacial
791 Melting Rates on the Younger Dryas Event and Deep-Ocean Circulation. *Nature* 342,
792 637-642.

793 Fernandes, M.B., Sicre, M.A., 2000. The importance of terrestrial organic carbon inputs on Kara
794 Sea shelves as revealed by n-alkanes, OC and $\delta^{13}\text{C}$ values. *Organic Geochemistry* 31,
795 363-374.

796 Fietz, S., Huguet, C., Rueda, G., Hambach, B., Rosell-Mele, A., 2013. Hydroxylated isoprenoidal
797 GDGTs in the Nordic Seas. *Marine Chemistry* 152, 1-10.

798 Gibson, J.A.E., Trull, T., Nichols, P.D., Summons, R.E., McMinn, A., 1999. Sedimentation of ¹³C-
799 rich organic matter from Antarctic sea-ice algae: A potential indicator of past sea-ice
800 extent. *Geology* 27, 331-334.

801 Haake, F.W., Pflaumann, U., 1989. Late Pleistocene Foraminiferal Stratigraphy on the Vøring
802 Plateau, Norwegian Sea. *Boreas* 18, 343-356.

803 Hald, M., Dokken, T., Mikalsen, G., 2001. Abrupt climatic change during the last interglacial-
804 glacial cycle in the polar North Atlantic. *Marine Geology* 176, 121-137.

805 Hall, A., 2004. The role of surface albedo feedback in climate. *Journal of Climate* 17, 1550-1568.

806 Haugan, P.M., 1999. Structure and heat content of the West Spitsbergen Current. *Polar*
807 *Research* 18 (2), 183-188.

808 Hebbeln, D., Dokken, T., Andersen, E.S., Hald, M., Elverhøi, A., 1994. Moisture supply for
809 northern ice-sheet growth during the Last Glacial Maximum. *Nature* 370, 357-359.

810 Hebbeln, D., Wefer, G., 1997. Late Quaternary paleoceanography in the Fram Strait.
811 *Paleoceanography* 12, 65-78.

812 Hedges, J.I., Clark, W.A., Quay, P.D., Richey, J.E., Devol, A.H., Santos, U.D.M., 1986.
813 Composition and fluxes of particulate organic material in the Amazon River. *Limnology*
814 *and Oceanography* 31, 717-738.

815 Henrich, R., 1998. Dynamics of Atlantic water advection to the Norwegian-Greenland Sea - time-
816 slice record of carbonate distribution in the last 300 ky. *Marine Geology* 145, 95-131.

817 Ho, S.L., Mollenhauer, G., Fietz, S., Martinez-Garcia, A., Lamy, F., Rueda, G., Schipper, K.,
818 Meheust, M., Rosell-Mele, A., Stein, R., Tiedemann, R., 2014. Appraisal of TEX₈₆ and
819 TEX₈₆^L thermometries in subpolar and polar regions. *Geochimica et Cosmochimica Acta*
820 131, 213-226.

821 Hörner, T., Stein, R., Fahl, K., Birgel, D., 2016. Post-glacial variability of sea ice cover, river run-
822 off and biological production in the western Laptev Sea (Arctic Ocean) - A high-resolution
823 biomarker study. *Quaternary Science Reviews* 143, 133-149.

824 Huang, W.Y., Meinschein, W.G., 1979. Sterols as ecological indicators. *Geochimica et*
825 *Cosmochimica Acta* 43(5), 739-745.

826 Hughes, A.L.C., Gyllencreutz, R., Lohne, Ø.S., Mangerud, J., Svendsen, J.I., 2016. The last
827 Eurasian ice sheets – a chronological database and time-slice reconstruction, DATED-1.
828 *Boreas* 45, 1-45.

829 Ingólfsson, Ó., Landvik, J.Y., 2013. The Svalbard-Barents Sea ice-sheet - Historical, current and
830 future perspectives. *Quaternary Science Reviews* 64, 33-60.

831 Ittekkot V., Haake, B., Bartsch, M., Nair, R.R., Ramaswamy, V., 1992. Organic carbon removal
832 in the sea: the continental connection. In: Prell, W.L., Emeis, K.C., Summerhayes, C.P.
833 (Eds.), *Upwelling systems: Evolution since the early Miocene*. Geological Society of
834 London, Special Publication 64, pp. 167-176.

835 Ivanov, V.V., Alexeev, V.A., Repina, I., Koldunov, N.V., Smirnov, A., 2012. Tracing Atlantic
836 Water Signature in the Arctic Sea Ice Cover East of Svalbard. *Advances in Meteorology*
837 2012, 11 pp.

838 Jaffé, R., Wolff, G.A., Cabrera, A.C., Carvajal-Chitty, H., 1995. The biogeochemistry of lipids in
839 rivers of the Orinoco Basin. *Geochimica et Cosmochimica Acta* 59, 4507-4522.

840 Jakobsson, M., Nilsson, J., O'Regan, M., Backman, J., Löwemark, L., Dowdeswell, J.A., Mayer, L.,
841 Polyak, L., Colleoni, F., Anderson, L., Björk, G., Darby, D., Eriksson, B., Hanslik, D., Hell, B.,
842 Marcussen, C., Sellén, E., Wallin, Å., 2010. An Arctic Ocean ice shelf during MIS 6
843 constrained by new geophysical and geological data. *Quaternary Science Reviews* 29,
844 3505-3517.

845 Jakobsson, M., Nilsson, J., Anderson, L., Backman, J., Björk, G., Cronin, T.M., Kirchner, N.,
846 Koshurnikov, A., Mayer, L., Noormets, R., O'Regan, M., Stranne, C., Ananiev, R., Macho,
847 N.B., Cherniykh, D., Coxall, H., Eriksson, B., Floden, T., Gemery, L., Gustafsson, O.,
848 Jerram, K., Johansson, C., Khortov, A., Mohammad, R., Semiletov, I., 2016. Evidence
849 for an ice shelf covering the central Arctic Ocean during the penultimate glaciation.
850 *Nature Communications* 7, 10365.

851 Jessen, S.P., Rasmussen, T.L., Nielsen, T., Solheim, A., 2010. A new Late Weichselian and
852 Holocene marine chronology for the western Svalbard slope 30,000-0 cal years BP.
853 *Quaternary Science Reviews* 29, 1301-1312.

854 Kim, J.H., Schouten, S., Hopmans, E.C., Donner, B., Damste, J.S.S., 2008. Global sediment
855 core-top calibration of the TEX₈₆ paleothermometer in the ocean. *Geochimica et*
856 *Cosmochimica Acta* 72, 1154-1173.

857 Kim, J.H., van der Meer, J., Schouten, S., Helmke, P., Willmott, V., Sangiorgi, F., Koc, N.,
858 Hopmans, E.C., Damste, J.S.S., 2010. New indices and calibrations derived from the
859 distribution of crenarchaeal isoprenoid tetraether lipids: Implications for past sea surface
860 temperature reconstructions. *Geochimica et Cosmochimica Acta* 74, 4639-4654.

861 King, J., Banerjee, S.K., Marvin, J., Özdemir, Ö., 1982. A comparison of different magnetic
862 methods for determining the relative grain size of magnetite in natural materials: Some
863 results from lake sediments. *Earth and Planetary Science Letters* 59(2), 404-419.

864 Knies, J., 1994. Spätquartäre Sedimentation am Kontinentalhang nordwestlich Spitzbergens.
865 Der letzte Glazial/Interglazial-Zyklus. Justus-Liebig-Universität, Gießen: 95 pp.
866 (unpublished diploma thesis).

867 Knies, J., Vogt, C., Stein, R., 1999. Late Quaternary growth and decay of the Svalbard/Barents
868 Sea ice sheet and paleoceanographic evolution in the adjacent Arctic Ocean. *Geo-*
869 *Marine Letters* 18, 195-202.

870 Knies, J., Nowaczyk, N., Müller, C., Vogt, C., Stein, R., 2000. A multiproxy approach to
871 reconstruct the environmental changes along the Eurasian continental margin over the
872 last 150 000 years. *Marine Geology* 163, 317-344.

873 Knies, J., Kleiber, H.-P., Matthiessen, J., Müller, C., Nowaczyk, N., 2001. Marine ice-rafted
874 debris records constrain maximum extent of Saalian and Weichselian ice-sheets along
875 the northern Eurasian margin. *Global and Planetary Change* 31, 45-64.

876 Knies, J., Hald, M., Ebbesen, H., Mann, U., Vogt, C., 2003. A deglacial-middle Holocene record
877 of biogenic sedimentation and paleoproductivity changes from the northern Norwegian
878 continental shelf. *Paleoceanography* 18, 1096.

879 Knies, J., Matthiessen, J., Vogt, C., Laberg, J.S., Hjelstuen, B.O., Smelror, M., Larsen, E.,
880 Andreassen, K., Eidvin, T., Vorren, T.O., 2009. The Plio-Pleistocene glaciation of the
881 Barents Sea-Svalbard region: a new model based on revised chronostratigraphy.
882 *Quaternary Science Reviews* 28, 812–829.

883 Knies, J., Stein, R., 1998. New aspects of organic carbon deposition and its paleoceanographic
884 implications along the northern Barents Sea margin during the last 30,000 years.
885 *Paleoceanography* 13, 384-394.

886 Knies, J., Vogt, C., 2003. Freshwater pulses in the eastern Arctic Ocean during Saalian and
887 Early Weichselian ice-sheet collapse. *Quaternary Research* 60, 243-251.

888 Landvik, J.Y., Bondevik, S., Elverhøi, A., Fjeldskaar, W., Mangerud, J., Salvigsen, O., Siegert,
889 M.J., Svendsen, J.I., Vorren, T.O., 1998. The last glacial maximum of Svalbard and the
890 Barents Sea area: Ice sheet extent and configuration. *Quaternary Science Reviews* 17,
891 43-75.

892 Landvik, J.Y., Brook, E.J., Gualtieri, L., Linge, H., Raisbeck, G., Salvigsen, O., Yiou, F., 2013.
893 ^{10}Be exposure age constraints on the Late Weichselian ice-sheet geometry and
894 dynamics in inter-ice-stream areas, western Svalbard. *Boreas* 42, 43-56.

895 Laskar, J., Robutel, P., Joutel, F., Gastineau, M., Correia, A., Levrard, B., 2004. A long-term
896 numerical solution for the insolation quantities of the Earth. *Astronomy & Astrophysics*
897 428, 261-285.

898 Lisiecki, L.E., Raymo, M.E., 2005. A Pliocene-Pleistocene stack of 57 globally distributed benthic
899 $\delta^{18}\text{O}$ records. *Paleoceanography* 20, PA1003.

900 Liu, X.L., Summons, R.E., Hinrichs, K.U., 2012. Extending the known range of glycerol ether
901 lipids in the environment: structural assignments based on tandem mass spectral
902 fragmentation patterns. *Rapid Communications in Mass Spectrometry* 26, 2295-2302.

903 Lloyd, J.M., Kroon, D., Boulton, G.S., Laban, C., Fallick, A., 1996. Ice rafting history from the
904 Spitsbergen ice cap over the last 200 kyr. *Marine Geology* 131, 103-121.

905 Lü, X.X., Liu, X.L., Elling, F.J., Yang, H., Xie, S.C., Song, J.M., Li, X.G., Yuan, H.M., Li, N.,
906 Hinrichs, K.U., 2015. Hydroxylated isoprenoid GDGTs in Chinese coastal seas and their
907 potential as a paleotemperature proxy for mid-to-low latitude marginal seas. *Organic*
908 *Geochemistry* 89-90, 31-43.

909 Mangerud, J., Jansen, E., Landvik, J.Y., 1996. Late Cenozoic history of the Scandinavian and
910 Barents Sea ice sheets. *Global and Planetary Change* 12, 11-26.

911 Mangerud, J., Dokken, T., Hebbeln, D., Heggen, B., Ingólfsson, O., Landvik, J.Y., Mejdahl, V.,
912 Svendsen, J.I., Vorren, T.O., 1998. Fluctuations of the Svalbard - Barents Sea Ice Sheet
913 during the last 150 000 years. *Quaternary Science Reviews* 17, 11-42.

914 Manley, T., Bourke, R., Hunkins, K., 1992. Near-surface circulation over the Yermak Plateau in
915 northern Fram Strait. *Journal of Marine Systems* 3, 107-125.

916 Manley, T., 1995. Branching of Atlantic Water within the Greenland-Spitsbergen Passage: An
917 estimate of recirculation. *Journal of Geophysical Research: Oceans* 100, 20627-20634.

918 Matthiessen, J., Knies, J., Nowaczyk, N.R., Stein, R., 2001. Late Quaternary dinoflagellate cyst
919 stratigraphy at the Eurasian continental margin, Arctic Ocean: indications for Atlantic
920 water inflow in the past 150,000 years. *Global and Planetary Change* 31, 65-86.

921 Matthiessen, J., Knies, J., 2001. Dinoflagellate cyst evidence for warm interglacial conditions at
922 the northern Barents Sea margin, during marine isotope stage 5. *Journal of Quaternary*
923 *Science* 16, 727-737.

924 Meyers, P.A., 1997. Organic geochemical proxies of paleoceanographic, paleolimnologic and
925 paleoclimatic processes. *Organic Geochemistry* 27, 213-250.

926 Müller, J., Massé, G., Stein, R., Belt, S.T., 2009. Variability of sea-ice conditions in the Fram
927 Strait over the past 30,000 years. *Nature Geoscience* 2, 772-776.

928 Müller, J., Wagner, A., Fahl, K., Stein, R., Prange, M., Lohmann, G., 2011. Towards quantitative
929 sea ice reconstructions in the northern North Atlantic: A combined biomarker and
930 numerical modelling approach. *Earth and Planetary Science Letters* 306, 137-148.

931 Müller, J., Werner, K., Stein, R., Fahl, K., Moros, M., Jansen, E., 2012. Holocene cooling
932 culminates in sea ice oscillations in Fram Strait. *Quaternary Science Reviews* 47, 1-14.

933 Müller, J., Stein, R., 2014. High-resolution record of late glacial and deglacial sea ice changes in
934 Fram Strait corroborates ice-ocean interactions during abrupt climate shifts. *Earth
935 and Planetary Science Letters* 403, 446-455.

936 Navarro-Rodriguez, A., Belt, S.T., Knies, J., Brown, T.A., 2013. Mapping recent sea ice
937 conditions in the Barents Sea using the proxy for palaeo sea ice reconstructions.
938 *Quaternary Science Reviews* 79, 26–39.

939 Niessen, F., Hong, J.K., Hegewald, A., Matthiessen, J., Stein, R., Kim, H., Kim, S., Jensen, L.,
940 Jokat, W., Nam, S.I., Kang, S.H., 2013. Repeated Pleistocene glaciation of the East
941 Siberian continental margin. *Nature Geoscience* 6, 842-846.

942 Nowaczyk, N.R., Frederichs, T.W., Eisenhauer, A., Gard, G., 1994. Magnetostratigraphic Data
943 from Late Quaternary Sediments from the Yermak Plateau, Arctic-Ocean - Evidence for 4
944 Geomagnetic Polarity Events within the Last 170 Ka of the Brunhes Chron. *Geophysical
945 Journal International* 117, 453-471.

946 O'Regan, M., King, J., Backman, J., Jakobsson, M., Pälike, H., Moran, K., Heil, C., Sakamoto,
947 T., Cronin, T.M., Jordan, R.W., 2008. Constraints on the Pleistocene chronology of
948 sediments from the Lomonosov Ridge. *Paleoceanography* 23, PA1S19.

949 Parkinson, C.L., Comiso, J.C., 2013. On the 2012 record low Arctic sea ice cover: Combined
950 impact of preconditioning and an August storm. *Geophysical Research Letters* 40, 1356–
951 1361.

952 Peeken, I., 2016. The Expedition PS92 of the Research Vessel POLARSTERN to the Arctic
953 Ocean in 2015. *Reports on Polar and Marine Research*, 694, 153 pp.

954 Polyak, L., Edwards, M.H., Coakley, B.J., Jakobsson, M., 2001. Ice shelves in the Pleistocene
955 Arctic Ocean inferred from glaciogenic deep-sea bedforms. *Nature* 410, 453-457.

956 Prah, F.G., Wakeham, S.G., 1987. Calibration of unsaturation pattern in long-chain ketone
957 compositions for paleotemperature assessment. *Nature* 330, 367-369.

958 Pryce, R.J., 1971. The occurrence of bound, water-soluble squalene, 4,4-dimethyl sterols, 4 α -
959 methyl sterols and sterols in leaves of *Kalanchoe blossfeldiana*. *Phytochemistry* 10,
960 1303-1307.

961 Rasmussen, T.L., Thomsen, E., 2008. Warm Atlantic surface water inflow to
962 the Nordic seas 34–10 cal. kyr B.P. *Paleoceanography* 23, PA1201.

963 Rasmussen, T.L., Bäckström, D., Heinemeier, J., Klitgaard-Kristensen, D., Knutz, P.C.,
964 Kuijpers, A., Lassen, S., Thomsen, E., Troelstra, S.R., van Weering, T.C.E., 2002. The
965 Faeroe – Shetland Gateway: Late Quaternary water mass exchange between the
966 Nordic seas and the northeastern Atlantic. *Mar. Geol.* 188, 165 – 192.

967 Rasmussen, T.L., Thomsen, E., 2008. Warm Atlantic surface water inflow to the Nordic seas 34
968 – 10 calibrated ka B.P. *Paleoceanography* 23, PA1201.

969 Reimer, P.J., Bard, E., Bayliss, A., Beck, J.W., Blackwell, P.G., Bronk, R.C., Buck, C.E., Cheng,
970 H., Edwards, R.L., Friedrich, M., 2013. IntCal13 and Marine13 radiocarbon age
971 calibration curves 0–50,000 years cal BP. *Radiocarbon* 55, 1869–1887.

972 Reimnitz, E., Dethleff, D., Nürnberg, D., 1994. Contrasts in Arctic Shelf Sea-Ice Regimes and
973 Some Implications - Beaufort Sea Versus Laptev Sea. *Marine Geology* 119, 215-225.

974 Robinson, N., Eglinton, G., Brassell, S.C., Cranwell, P.A., 1984. Dinoflagellate Origin for
975 Sedimentary 4 α -Methylsteroids and 5 α (*H*)-Stanols. *Nature* 308, 439-442.

976 Rontani, J.F., Charrière, B., Sempéré, R., Doxaran, D., Vaultier, F., Vonk, J.E., Volkman, J.K.,
977 2014. Degradation of sterols and terrigenous organic matter in waters of the Mackenzie
978 Shelf, Canadian Arctic. *Organic Geochemistry* 75, 61-73.

979 Rowland, S.J., Allard, W.G., Belta, S.T., Massae, G., Robert, J.M., Blackburn, S., Frampton, D.,
980 Revill, A.T., Volkman, J.K., 2001. Factors influencing the distributions of polyunsaturated
981 terpenoids in the diatom, *Rhizosolenia setigera*. *Phytochemistry* 58, 717-728.

982 Ruddiman, W.F., McIntyre, A., 1981. Oceanic Mechanisms for Amplification of the 23,000-Year
983 Ice-Volume Cycle. *Science* 212, 617-627.

984 Rudels, B., Friedrich, H.J., Quadfasel, D., 1999. The Arctic circumpolar boundary current. *Deep
985 Sea Research Part II: Topical Studies in Oceanography* 46, 1023-1062.

986 Rutgers van der Loeff, M.M., Meyer, R., Rudels, B., Rachor, E., 2002. Resuspension and
987 particle transport in the benthic nepheloid layer in and near Fram Strait in relation to
faunal abundance and ²³⁴Th depletion. *Deep Sea Research* 149, 1941-1958.

988 Sachs J.P., Pahnke K., Smittenberg R., Zhang Z., 2013. Biomarker Indicators of Past Climate.
989 In: Elias, S.A. (Eds.), The Encyclopedia of Quaternary Science. Elsevier, Amsterdam, pp.
990 775-782.

991 Sakshaug, E., 2004. Primary and secondary production in the Arctic Seas. In: Stein, R.,
992 Macdonald, R.W. (Eds.), The organic carbon cycle in the Arctic Ocean. Springer, Berlin,
993 pp. 57-82.

994 Sarnthein, M., Pflaumann, U., Weinelt, M., 2003. Past extent of sea ice in the northern North
995 Atlantic inferred from foraminiferal paleotemperature estimates. *Paleoceanography*
996 18(2), 25-1-25-8.

997 Sarnthein, M., Werner, K., 2017. Early Holocene planktic foraminifers record species-specific ¹⁴C
998 reservoir ages in Arctic Gateway. *Marine Micropaleontology* 135, 45-55.

999 Scheffer, F., Schachtschabel, P., 1984. Lehrbuch der Bodenkunde. Enke Verlag, Stuttgart, 442
1000 pp.

1001 Schouten, S., Hopmans, E.C., Schefuß, E., Sinninghe Damsté, J.S., 2002. Distributional
1002 variations in marine crenarchaeotal membrane lipids: A new tool for reconstructing
1003 ancient sea water temperatures? *Earth Planetary Science Letters* 204, 265-274.

1004 Serreze, M.C., Holland, M.M., Stroeve, J., 2007. Perspectives on the Arctic's shrinking sea ice
1005 cover. *Science* 315, 1533–1536.

1006 Serreze, M.C., Barry, R.G., 2011. Processes and impacts of Arctic amplification: A research
1007 synthesis. *Global and Planetary Change* 77, 85-96.

1008 Smik, L., Cabedo-Sanz, P., Belt, S.T., 2016. Semi-quantitative estimates of paleo Arctic sea ice
1009 concentration based on source-specific highly branched isoprenoid alkenes: A further
1010 development of the PIP₂₅ index. *Organic Geochemistry* 92, 63-69.

1011 Smith, W.O., 1987. Phytoplankton Dynamics in Marginal Ice Zones. *Oceanography and Marine*
1012 *Biology* 25, 11-38.

1013 Soltwedel, T., Mokievsky, V., Schewe, I., 2000. Benthic activity and biomass on the Yermak
1014 Plateau and in adjacent deep-sea regions northwest of Svalbard. *Deep-Sea*
1015 *Research Part I*, 47, 1761-1785.

1016 Spielhagen, R.F., 1991. Die Eisdrift in der Framstraße während der letzten 200.000 Jahre.
1017 GEOMAR Report, Kiel (GEOMAR, Kiel), 4: 133 pp.

1018 Spielhagen, R.F., Baumann, K.H., Erlenkeuser, H., Nowaczyk, N.R., Norgaard-Pedersen, N.,
1019 Vogt, C., Weiel, D., 2004. Arctic Ocean deep-sea record of northern Eurasian ice sheet
1020 history. *Quaternary Science Reviews* 23, 1455-1483.

1021 Stein, R., Grobe, H., Wahsner, M., 1994. Organic-Carbon, Carbonate, and Clay Mineral
1022 Distributions in Eastern Central Arctic-Ocean Surface Sediments. *Marine Geology* 119,
1023 269-285.

1024 Stein, R., Boucsein, B., Fahl, K., Garcia de Oteyza, T., Knies, J., Niessen, F., 2001.
1025 Accumulation of particulate organic carbon at the Eurasian continental margin during late
1026 Quaternary times: Controlling mechanisms and paleoenvironmental significance. *Global
1027 and Planetary Change* 31, 87-104.

1028 Stein, R., Fahl, K., Müller, J., 2012. Proxy reconstruction of Arctic Ocean sea ice history: from
1029 IRD to IP₂₅. *Polarforschung* 82, 37-71.

1030 Stein, R., Fahl, K., Schreck, M., Knorr, G., Niessen, F., Forwick, M., Gebhardt, C., Jensen, L.,
1031 Kaminski, M., Kopf, A., Matthiessen, J., Jokat, W., Lohmann, G., 2016. Evidence for ice-
1032 free summers in the late Miocene central Arctic Ocean. *Nature Communications* 7, 1-13.

1033 Stein, R., Fahl, K., Schade, I., Manerung, A., Wassmuth, S., Niessen, F., Nam, S., 2017a.
1034 Holocene variability in sea ice cover, primary production, and Pacific-Water inflow and
1035 climate change in the Chukchi and East Siberian Seas (Arctic Ocean). *Journal of
1036 Quaternary Science* 32, 362-379.

1037 Stein, R., Fahl, K., Gierz, P., Niessen, F., Lohmann, G., 2017b. Arctic Ocean sea ice cover
1038 during the penultimate glacial and the last interglacial. *Nature Communications* 8, 373.

1039 Stein, R., Fahl, K., 2013. Biomarker proxy shows potential for studying the entire Quaternary
1040 Arctic sea ice history. *Organic Geochemistry* 55, 98-102.

1041 Stein, R., Macdonald, R.W., 2004. Geochemical Proxies Used for Organic Carbon Source
1042 Identification in Arctic Ocean Sediments. In: Stein, R., Macdonald, R.W. (Eds.), *The
1043 Organic Carbon Cycle in the Arctic Ocean*, Springer-Verlag, Berlin, pp. 24-32.

1044 Steinsund, P.I., Hald, M., 1994. Recent Calcium-Carbonate Dissolution in the Barents Sea -
1045 Paleoceanographic Applications. *Marine Geology* 117, 303-316.

1046 Stuiver, M., Braziunas, T.F., 1993. Modeling atmospheric ¹⁴C influences and ¹⁴C ages of marine
1047 samples to 10,000 BC. *Radiocarbon* 35, 137-189.

1048 Stuiver, M., Reimer, P.J., 1993. Extended ¹⁴C Data-Base and Revised Calib 3.0 ¹⁴C Age
1049 Calibration Program. *Radiocarbon* 35, 215-230.

1050 Svendsen, J.I., Alexanderson, H., Astakhov, V.I., Demidov, I., Dowdeswell, J.A., Funder, S.,
1051 Gataullin, V., Henriksen, M., Hjort, C., Houmark-Nielsen, M., Hubberten, H.W.,
1052 Ingolfsson, O., Jakobsson, M., Kjaer, K.H., Larsen, E., Lokrantz, H., Lunkka, J.P., Lysa,
1053 A., Mangerud, J., Matiouchkov, A., Murray, A., Moller, P., Niessen, F., Nikolskaya, O.,

1054 Polyak, L., Saarnisto, M., Siebert, C., Siebert, M.J., Spielhagen, R.F., Stein, R., 2004.
1055 Late Quaternary ice sheet history of northern Eurasia. *Quaternary Science Reviews* 23,
1056 1229-1271.

1057 Thompson, W.G., Goldstein, S.L., 2006. A radiometric calibration of the SPECMAP timescale.
1058 *Quaternary Science Reviews* 25, 3207–3215.

1059 Vinje, T., 2001. Anomalies and trends of sea-ice extent and atmospheric circulation in the Nordic
1060 Seas during the period 1864-1998. *Journal of Climate* 14, 255-267.

1061 Vogt, C., 1997. Regional and temporal variations of mineral assemblages in Arctic Ocean
1062 sediments as climatic indicator during glacial/interglacial changes. *Reports on Polar*
1063 *Research* 251, 1-309.

1064 Vogt, P.R., Crane, K., Sundvor, E., 1994. Deep Pleistocene Iceberg Plowmarks on the Yermak
1065 Plateau - Sidescan and 3.5 Khz Evidence for Thick Calving Ice Fronts and a Possible
1066 Marine Ice-Sheet in the Arctic-Ocean. *Geology* 22, 403-406.

1067 Vogt, C., Knies, J., Spielhagen, R.F., Stein, R., 2001. Detailed mineralogical evidence for two
1068 nearly identical glacial/deglacial cycles and Atlantic water advection to the Arctic Ocean
1069 during the last 90,000 years. *Global and Planetary Change* 31, 23-44.

1070 Volkman, J.K., 1986. A Review of Sterol Markers for Marine and Terrigenous Organic-Matter.
1071 *Organic Geochemistry* 9, 83-99.

1072 Volkman, J.K., Barrett, S.M., Blackburn, S.I., Mansour, M.P., Sikes, E.L., Gelin, F., 1998.
1073 Microalgal biomarkers: A review of recent research developments. *Organic Geochemistry*
1074 29, 1163-1179.

1075 Volkman, J.K., 2006. Lipid markers for marine organic matter. In: Volkman, K., (Eds.), *Marine*
1076 *Organic Matter: Biomarkers, Isotopes and DNA*. Springer, Berlin, pp. 27-70.

1077 Volkman, J.K., Revill, A.T., Holdsworth, D.G., Fredericks, D., 2008. Organic matter sources in an
1078 enclosed coastal inlet assessed using lipid biomarkers and stable isotopes. *Organic*
1079 *Geochemistry* 39 (6), 689-710.

1080 Winkelmann, D., Schafer, C., Stein, R., Mackensen, A., 2008a. Terrigenous events and climate
1081 history of the Sophia Basin, Arctic Ocean. *Geochemistry Geophysics Geosystems* 9,
1082 Q07023.

1083 Winkelmann, D., Geissler, W., Schneider, J., Stein, R., Schenke, H.-W., 2008b. Dynamics and
1084 timing of the Hinlopen/Yermak Megaslide north of Spitsbergen, Arctic Ocean. *Marine*
1085 *Geology* 250, 34–50.

1086 Wollenburg, J.E., Kuhnt, W., Mackensen, A., 2001. Changes in Arctic Ocean paleoproductivity
1087 and hydrography during the last 145 kyr: The benthic foraminiferal record.
1088 *Paleoceanography* 16, 65-77.

1089 Xiao, X.T., Fahl, K., Müller, J., Stein, R., 2015a. Sea-ice distribution in the modern Arctic Ocean:
1090 Biomarker records from trans-Arctic Ocean surface sediments. *Geochimica et*
1091 *Cosmochimica Acta* 155, 16-29.

1092 Xiao, X.T., Stein, R., Fahl, K., 2015b. MIS 3 to MIS 1 temporal and LGM spatial variability in
1093 Arctic Ocean sea ice cover: Reconstruction from biomarkers. *Paleoceanography* 30, 969-
1094 983.

1095 Xuan, C., Channell, J.E.T., Polyak, L., Darby, D.A., 2012. Paleomagnetism of Quaternary
1096 sediments from Lomonosov Ridge and Yermak Plateau: implications for age models in
1097 the Arctic Ocean. *Quaternary Science Reviews* 32, 48-63.

1098

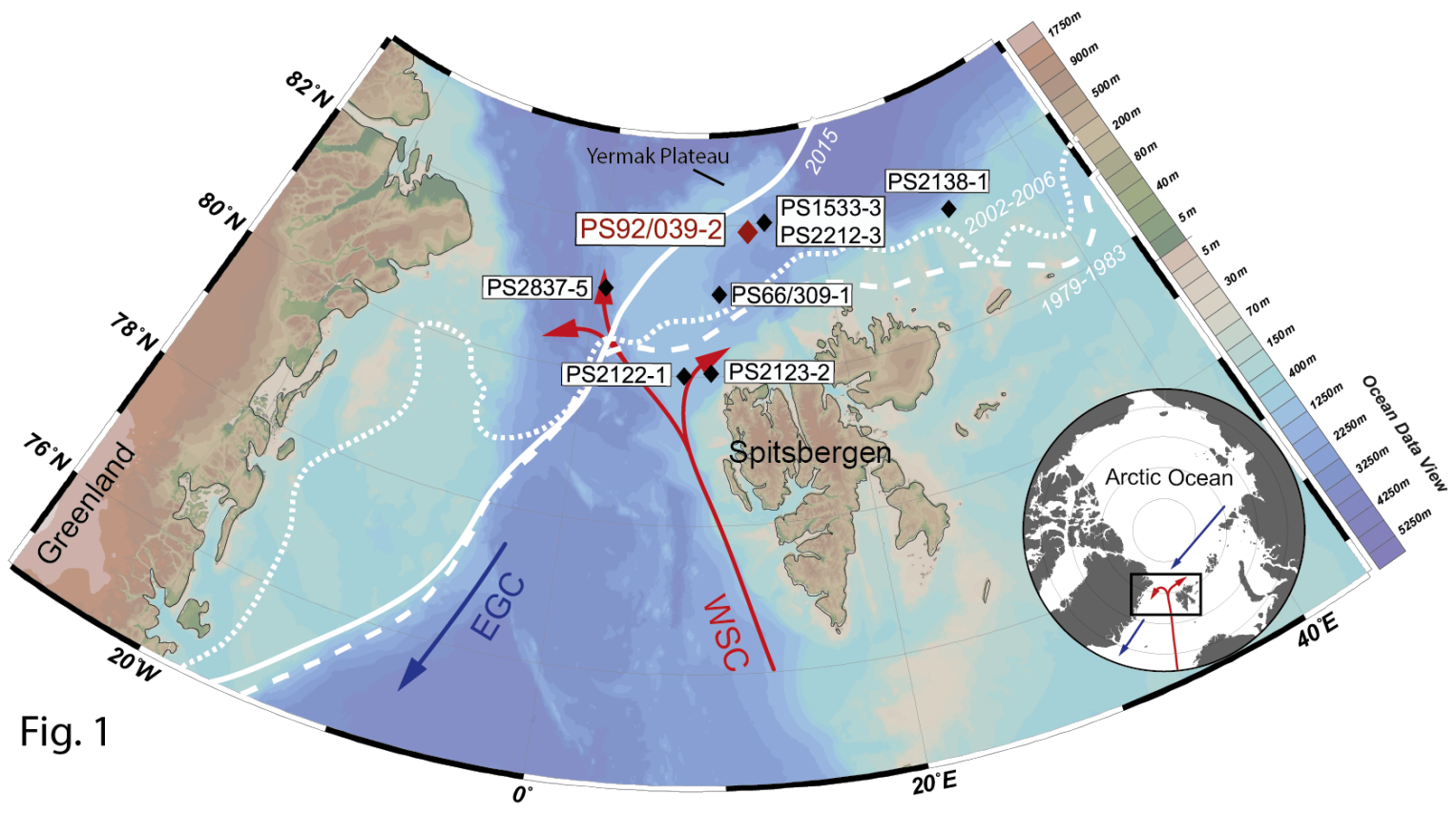


Fig. 1

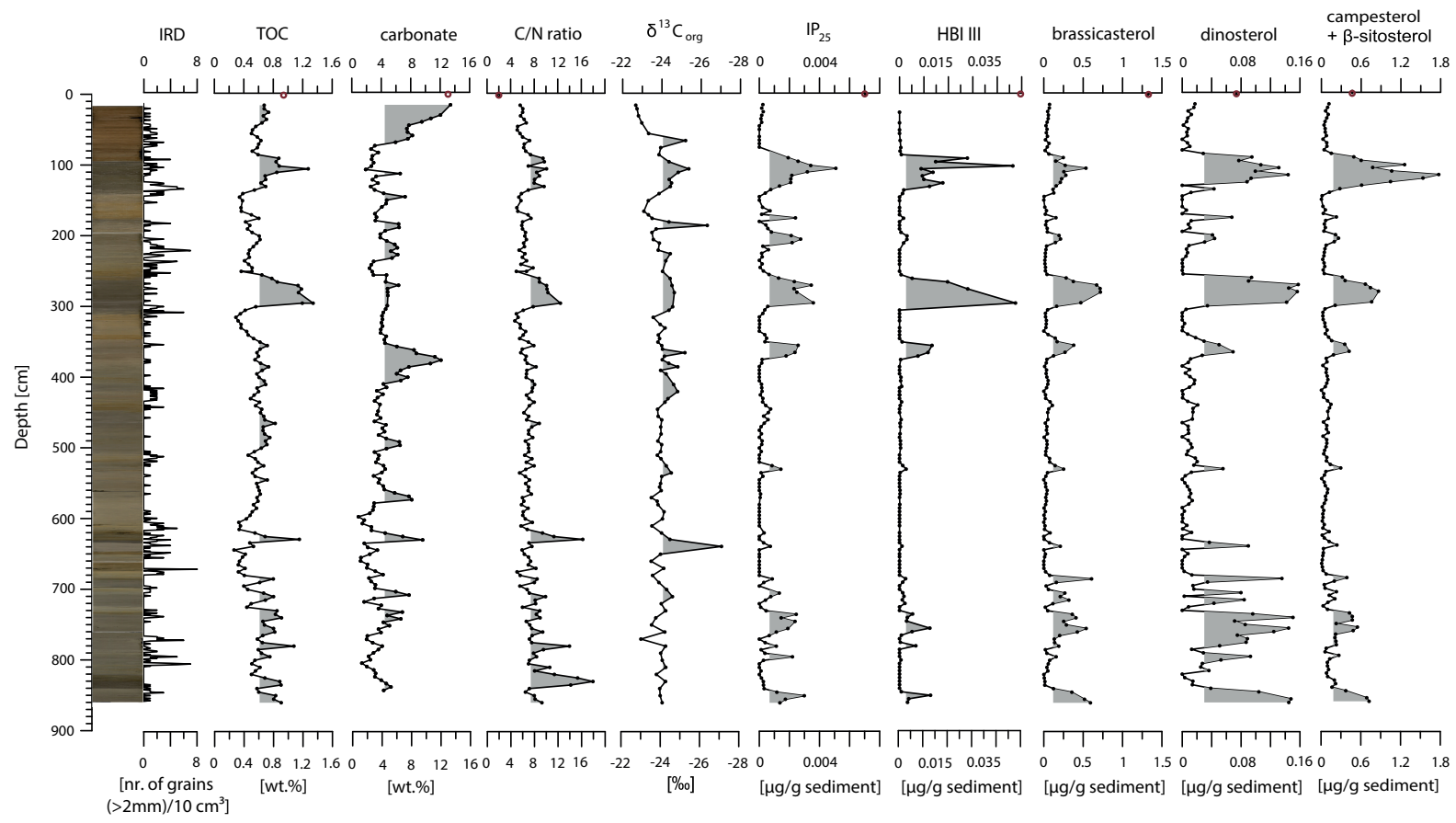


Fig. 2

PS92/039-2

PS1533-3

Global

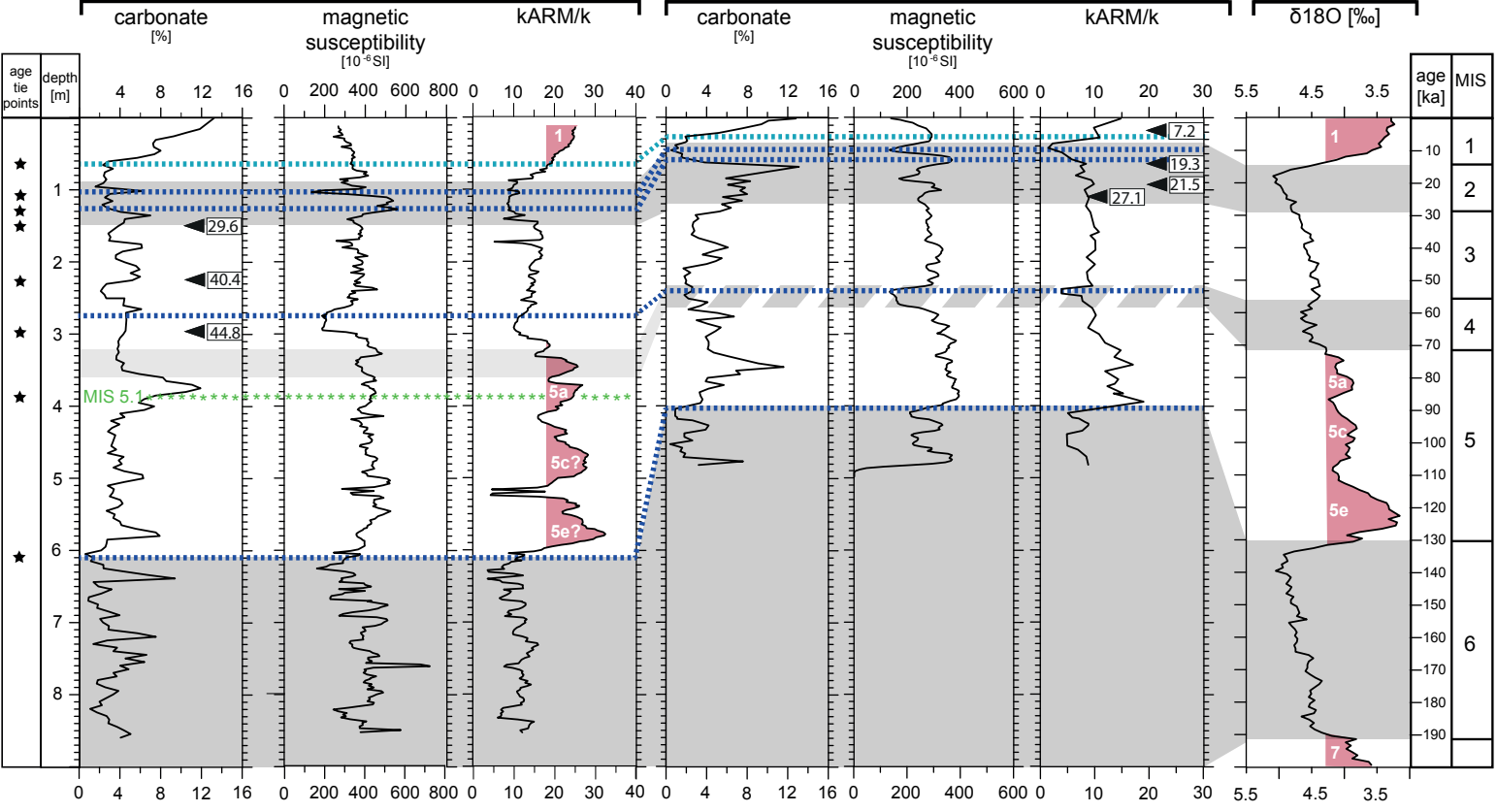


Fig. 3

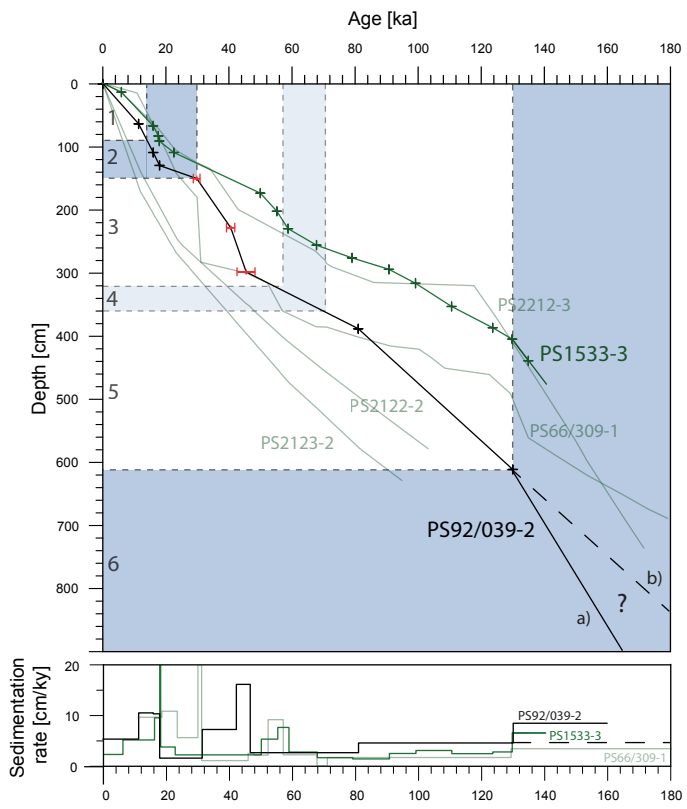


Fig. 4

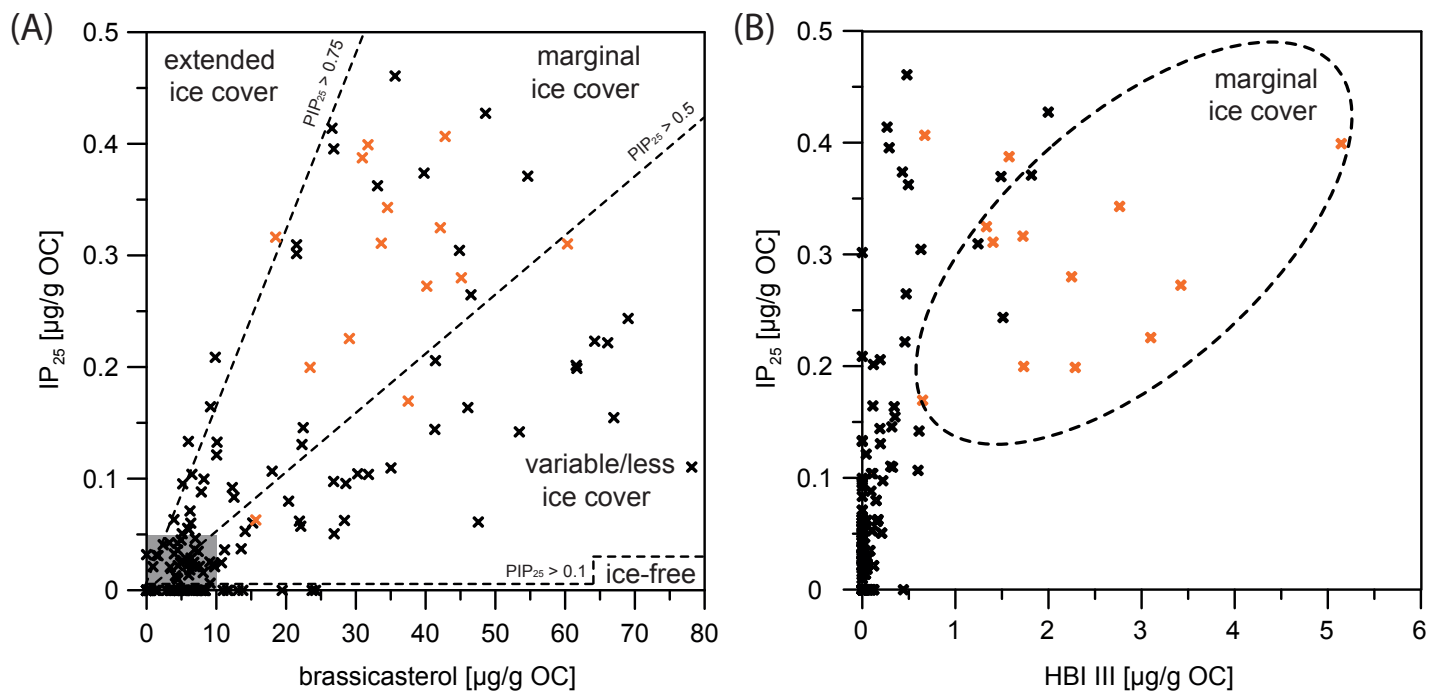


Fig. 5

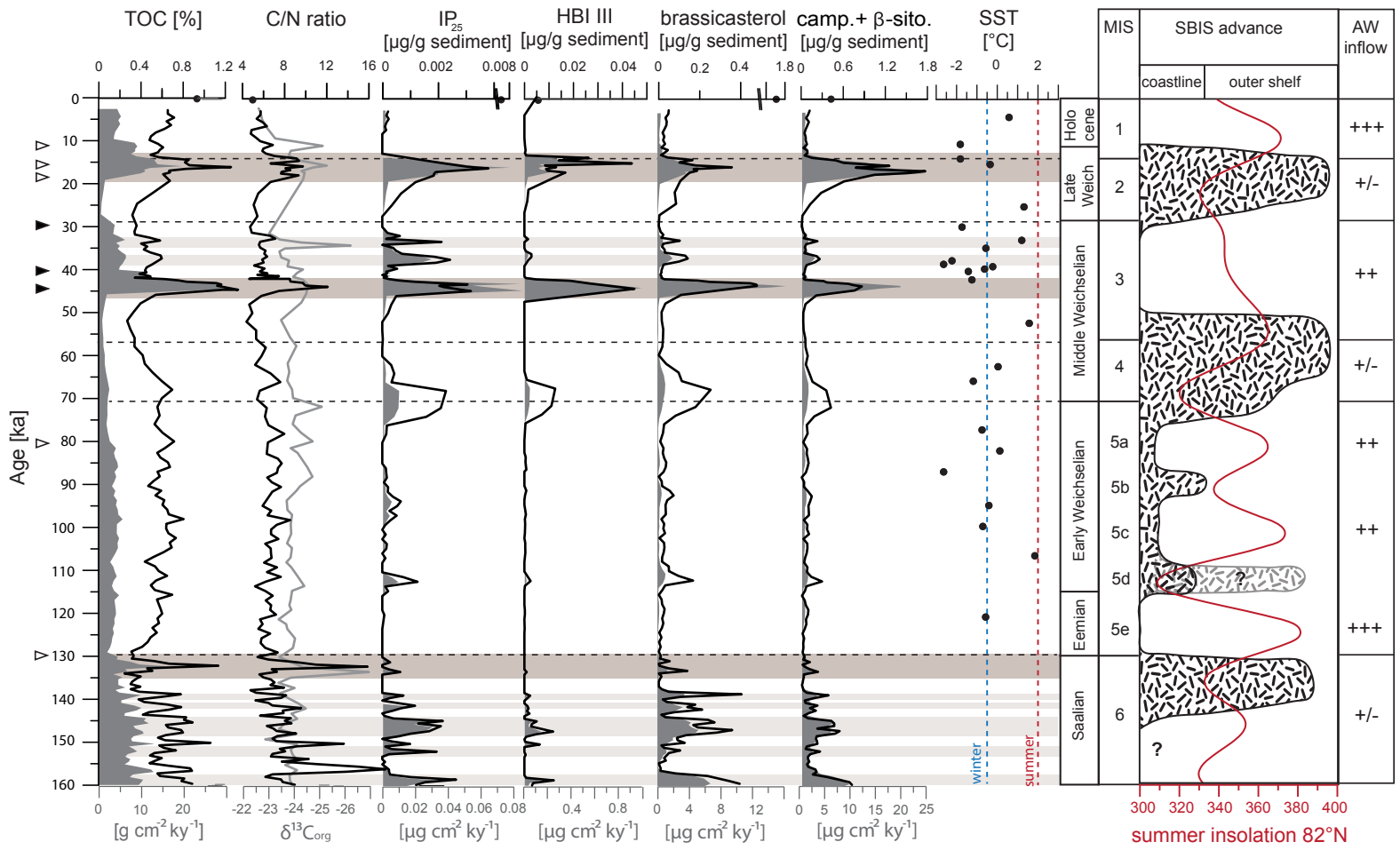


Fig. 6

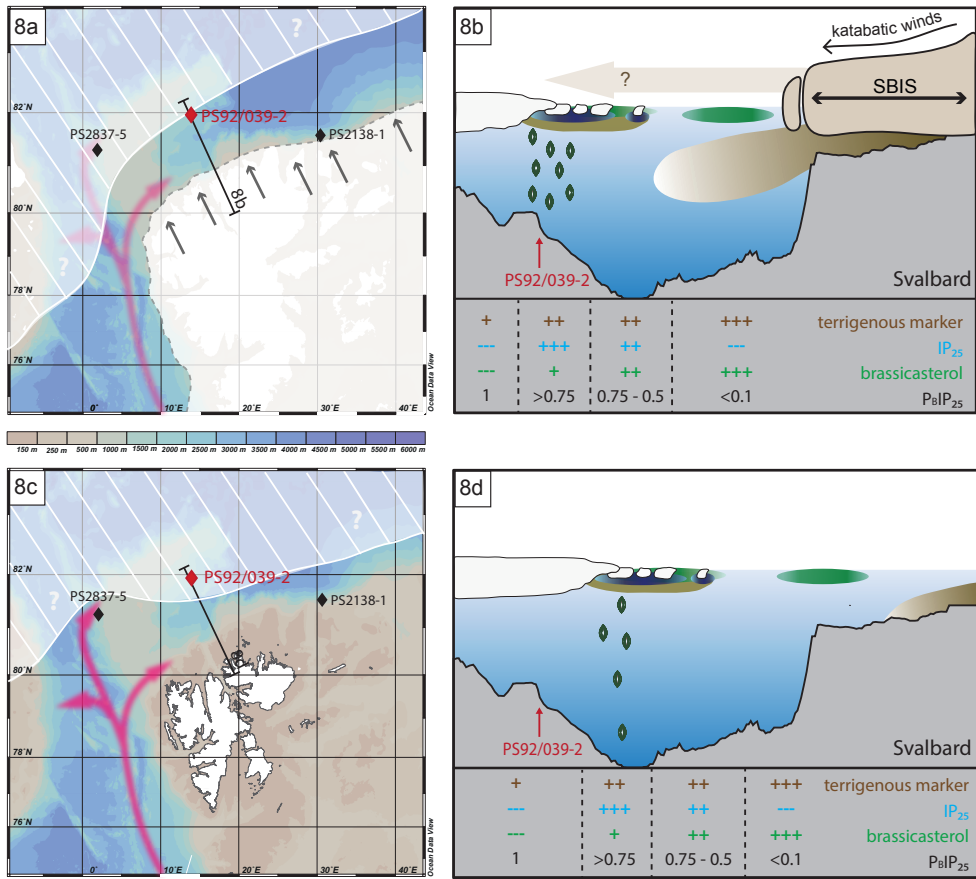


Fig. 8

Fig. 1. Overview map of the Arctic Ocean (inset) and the oceanographic setting in the study area. The red arrow refers to the West Spitsbergen Current (WSC), the blue arrow indicates the East Greenland Current (EGC). The position of the September sea ice margin for the time intervals 1979 – 1983 and 2002 – 2006 is marked by white, dotted lines, the sea ice extent during September 2015 is indicated by a white, solid line (<http://iup.physik.uni-bremen.de>). Core locations are marked by diamonds, the herein investigated Core PS92/039-2 is highlighted in red.

Fig. 2. Line-scan image, bulk parameter contents (IRD [nr. of grains (>2mm)/10 cm³], TOC [wt.%], carbonate [wt.%], C/N ratio, $\delta^{13}\text{C}_{\text{org}}$ [‰]) and biomarker contents (IP₂₅ [$\mu\text{g/g}$ sediment], HBI III [$\mu\text{g/g}$ sediment], brassicasterol [$\mu\text{g/g}$ sediment], dinosterol [$\mu\text{g/g}$ sediment], sum of terrigenous sterols: campesterol and β -sitosterol [$\mu\text{g/g}$ sediment]) of Core PS92/039-2 and Core PS92/039-3 (surface sample, red dot) against depth [cm]. Note that brassicasterol and dinosterol are moving synchronously and that brassicasterol is henceforth used as representative for the phytoplankton sterols. Grey shading highlights values lying above the mean.

Fig. 3. Stratigraphic framework of Core PS92/039-2. The age tie points (black asterisks) derive from: the correlation of (1) a significant decrease in the carbonate content (light blue, dashed line), (2) a minimum followed by (3) a maximum in the magnetic susceptibility record (blue, dashed lines) to corresponding values at nearby Core PS1533-3 (Spielhagen et al., 2004), (4, 5, 6) radiocarbon ages (indicated as calibrated dates; ka B.P.), (7) the identification of *Pullenia bulloides* as stratigraphic marker for MIS event 5.1 (green asterisks; Haake and Pflaumann, 1989) and (8) a distinct decrease in the magnetic susceptibility correlated to Core PS1533-3 (Spielhagen et al., 2004). An additional, independent confirmation of the age model is given by the correlation of the kARM/k ratio of Core PS92/039-2 to the global benthic $\delta^{18}\text{O}$ record of Lisiecki and Raymo (2005). The kARM/k

ratio of Core PS1533-3 is indicated for comparability (Nowaczyk et al., 1994). Interglacial minima in the global benthic $\delta^{18}\text{O}$ stack are highlighted in red colouration and transferred to the kARM/k ratio of Core PS92/039-2. The ages of MIS boundaries are adopted in accordance to Lisiecki and Raymo (2005) and Thompson and Goldstein (2006) with grey shading referring to glacial intervals. The grey, hatched area indicates the sediment sequence identified as MIS 4 in the original age model of Core PS1533-3 (Spielhagen et al., 2004). The positions of the stage boundaries of MIS 4 in Core PS92/039-2 were calculated using linear interpolation and have to be considered as possible insecurity.

Fig. 4. Age-depth model and sedimentation rates [cm/ky] for the cores PS92/039-2 (black), PS1533-3 (green, green crosses indicate age tie points) and PS2123-3, PS2122-2, PS2212-3, PS66/309-1 (pale print). Calibrated radiocarbon dates with error bars are highlighted in red. Black crosses indicate age tie points obtained from biostratigraphy and correlation of the carbonate and magnetic susceptibility records to nearby Core PS1533-3 (Spielhagen et al., 2004). A linear interpolation is used to calculate ages in between these age tie points. MIS boundaries (according to Lisiecki and Raymo [2005] and Thompson and Goldstein [2006]) are indicated by dashed lines, blue shading refers to glacial intervals. The positions of the stage boundaries for MIS 4 were calculated using a linear interpolation and have to be considered as possible insecurity. According to linear extrapolation, the age of the core base is ~180 ka (option b). However, previous studies north of Spitsbergen described significantly higher sedimentation rates in MIS 6 compared to the following MIS 5 interval (Knies et al., 2001; Stein et al., 2001; Winkelmann et al., 2008). Assuming similar changes for Core PS92/039-2, the more probable age of the core base is ~160 ka (option a).

Fig. 5. IP_{25} [$\mu\text{g/g OC}$] versus (A) brassicasterol [$\mu\text{g/g OC}$] and (B) HBI III [$\mu\text{g/g OC}$]. The classification of the different sea ice scenarios refers to Müller et al. (2011). The grey rectangle indicates PIP_{25} values of 1, representative for a permanent sea ice cover. As there

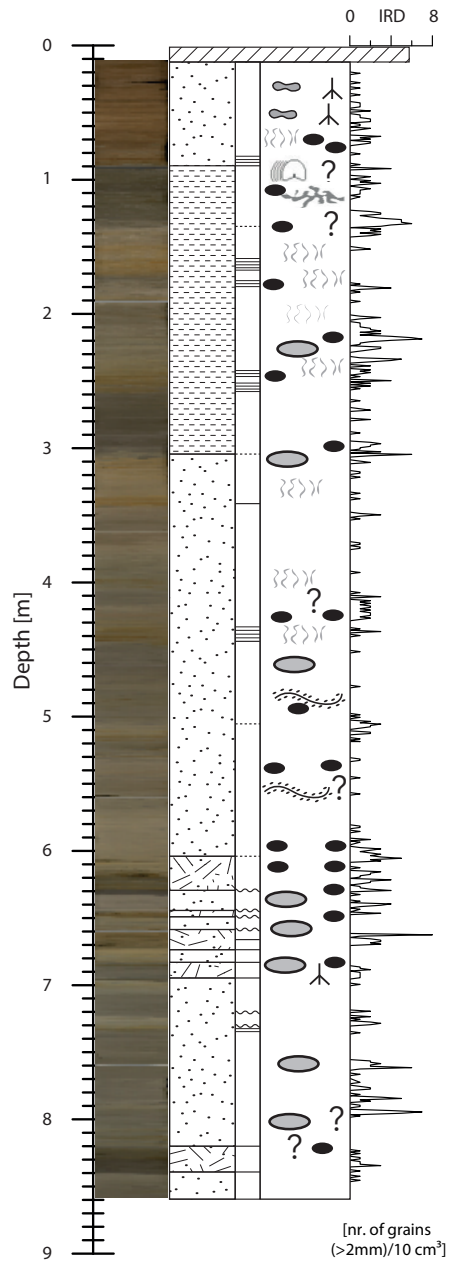
is no empirical correlation between the $P_{III}IP_{25}$ index and sea ice conditions so far, a comparable relation was assumed and the categorisation of Müller et al. (2011) adopted. Orange crosses indicate data points from intervals of enhanced organic carbon accumulation on the Yermak Plateau.

















Fig. 6. Fluctuations of the TOC content [wt.%], $\delta^{13}C_{org}$ values [‰], the C/N ratio and the biomarker concentrations [$\mu\text{g/g}$ sediment] against age [ka]. Accumulation rates of TOC [$\text{g cm}^{-2} \text{ky}^{-1}$] and the biomarkers [$\mu\text{g cm}^{-2} \text{ky}^{-1}$] are indicated as grey colouration. Note that the core age of ~ 160 ka is based on the assumption that the change in sedimentation rate between MIS 5 and MIS 6 is similar to observations in adjacent cores (Knies et al., 2001; Stein et al., 2001, Winkelmann et al., 2008). Age tie points are indicated by triangles, filled triangles represent calibrated radiocarbon ages. Brown shading refers to sequences of synchronously enhanced contents of terrigenous organic carbon, IP_{25} , the phytoplankton markers (brassicasterol, HBI III) and the terrigenous sterols (β -sitosterol, campesterol), whereby the darker colour highlights the most conspicuous intervals. OH-GDGT-based SST estimates (after Lü et al., 2015) in the range of -2.5 to 2.5°C highlight the throughout close proximity to the sea ice margin. Today's mean summer and winter SSTs in the study area are indicated by dashed red and blue lines, respectively (cf., Sarnthein et al., 2003). On the right side, the summer insolation at 82°N (Laskar et al., 2004), the extent of the Svalbard Barents Sea Ice Sheet (SBIS; Mangerud et al., 1998; Winkelmann et al., 2008) and the inflow strength of Atlantic Water (Spielhagen et al., 2004) are illustrated for the last 160,000 years.

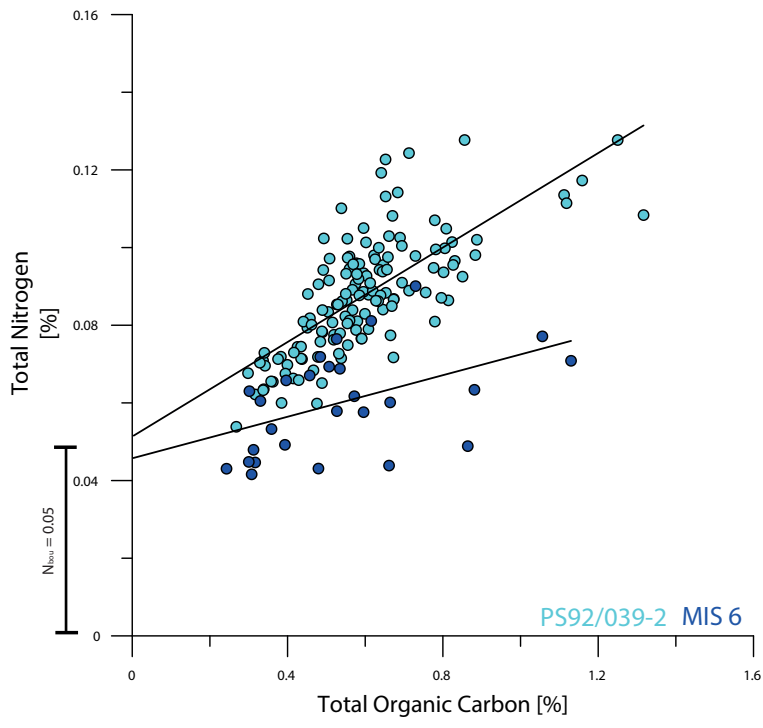
Fig. 7. PIP_{25} indices for Core PS92/039-2 from the eastern Yermak Plateau over the last 160,000 years. Note that the core age of ~ 160 ka is based on the assumption that the change in sedimentation rate between MIS 5 and MIS 6 is similar to observations in adjacent cores (Knies et al., 2001; Stein et al., 2001, Winkelmann et al., 2008). P_BIP_{25} indices are calculated using the sterol brassicasterol as phytoplankton marker, while $P_{III}IP_{25}$ indices

include the tri-unsaturated HBI III as open water counterpart. The coloured area displays the floating average of three data points. The classification of the different sea ice scenarios refers to Müller et al. (2011), whereby the dark to light grey shading indicates the transition from extended to less sea ice cover. As there is no empirical correlation between the $P_{III}IP_{25}$ index and sea ice conditions so far, a comparable relation was assumed and the categorisation of Müller et al. (2011) adopted. Age tie points are indicated by triangles, filled triangles represent calibrated radiocarbon ages. For the last 40 ka, a comparison with $P_{B}IP_{25}$ indices for Core PS2837-5 from the western Yermak Plateau is given (Müller et al., 2009).

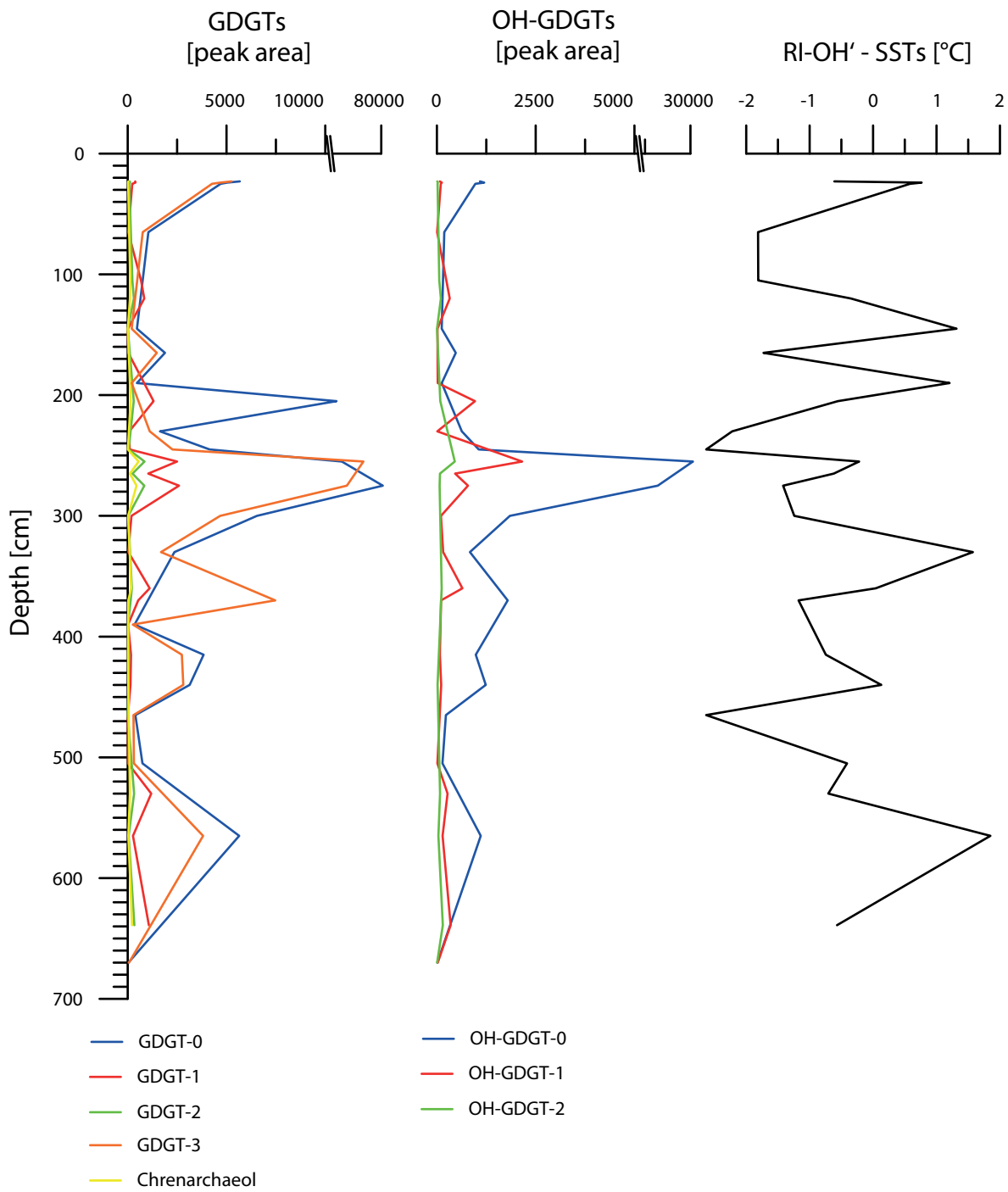
Fig. 8. Overview map and schematic illustration of the sedimentation regime along a transect from the northern coast of Svalbard to the Yermak Plateau (black line) for different settings: (8a, b) scenario for full glacial conditions with major glaciation on Svalbard and (8c, d) scenario for interglacial conditions with no glaciation on Svalbard. The core position of Core PS92/039-2 is indicated in red. The white shading in 8a refers to the extent of the Svalbard Barents Sea Ice Sheet (SBIS), the white crosshatched shading indicates the potential sea ice extent. The thick, light arrow in 8b illustrates the hypothesised advance of the SBIS during MIS 6 that could not be unambiguously identified in the biomarker records of PS92/039-2. Red arrows indicate Atlantic Water entering the Arctic Ocean via the Fram Strait. Blue, green and brown shadings in 8b and 8d mark the input of ice algae, open-water phytoplankton and terrigenous material, respectively. The related sedimentary contents of IP_{25} , the phytoplankton markers and the terrigenous markers as well as $P_{B}IP_{25}$ indices are indicated.



-  Biodeformational structures
-  Chondrites-like
-  Planolites-like (small)
-  Planolites-like (large)
-  Phycosiphon
-  Nereites-like burrows
-  Trichichnus
-  Scolicia
-  diamicton
-  clay
-  mud
-  disturbed
-  transitional contact
-  wavy contact
-  sharp contact
-  lamination



Supplementary Fig. 2



Supplementary Fig. 3

Supplementary Fig. 1. Line-scan image, illustrated core description, ichnofossils and IRD counts of Core PS92/039-2. In the lowermost part of the core (860 - 615 cm), the dominant lithotypes are silty clays intercalated by diamicton layers. An alternation of greyish, dark greyish and brownish coloured intervals can be observed. The overlaying sequence from 615 to 90 cm consists of clayey to silty clayey sediments with a greyish to brownish colour spectrum. Two layers of dark greyish colouration are conspicuous between 310 - 260 cm and 140 - 90 cm. The upper 90 cm are composed of brownish sediments. Various bioturbation traces are present throughout the entire record, except for short intervals around 730, 580, 510, 365 and 275 cm. Peak abundance of IRD can be observed in the intervals 650 - 600, 250 - 200 and 145 - 120 cm, while only minor IRD grains are found in 590 - 310 cm core depth.

Supplementary Fig. 2. Total nitrogen (TN) versus total organic carbon (TOC) correlation for Core PS92/039-2. The C/N ratio was calculated using the TOC and TN contents, thereby neglecting the inorganic nitrogen (N_{bou}) portion (cf., Stein and Macdonald, 2004). As there is an intercept of $\sim 0.05\%$ TN at 0% TOC, the presence of a significant proportion of inorganic nitrogen is likely (cf., Stein and Macdonald, 2004). The large scatter of data points, especially including the MIS 6 interval (in blue) that is characterised by generally smaller TN values and therefore relatively high N_{bou} proportions, impedes a N_{bou} correction. Hence, the C/N values of Core PS92/039-2 may be smaller compared to reference values (e.g., Bordowskiy, 1965; Scheffer and Schachtschabel, 1984; Hedges et al., 1986), leading to an underestimation of the terrigenous proportion of organic matter. However, relative changes of the ratio can still be used to estimate the input of terrigenous versus marine organic matter.

Supplementary Fig. 3. Peak areas of GDGTs and OH-GDGTs against depth. SSTs ($^{\circ}\text{C}$) were calculated using the RI-OH' index recommended for polar regions (Lü et al., 2015). The TEX_{86}^L index was not used in this study as it revealed unrealistic temperatures.

Table 1. Investigated cores.

Core-ID	Latitude [°N]	Longitude [°E]	Water depth [m]	Core recovery [cm]
PS92/039-2 KAL	81.95	13.83	1464	860
PS92/039-3 GKG	81.94	13.75	1493	43

Table 2. Results of AMS¹⁴C.

Lab-ID	Depth [cmbsf]	Material	Corrected Ages, ¹⁴ C years	Calibrated Ages
BETA 452275	150	<i>N.pachyderma</i> sin.	28240±140 BP	29589
BETA 425247	227.5	<i>N.pachyderma</i> sin.	38550±520 BP	40367
NTUAMS-3357	298	<i>N.pachyderma</i> sin.	44187±2900 BP	44782

Radiocarbon dates were corrected for a reservoir effect of 400 years (Stuiver and Braziunas, 1993; Sarnthein and Werner, 2017) and converted to calendar ages (ka) using the CALIB 7.1 calibration program and the “Marine 13” calibration data set (Stuiver and Reimer, 1993; Reimer et al., 2013).

Table 3. Age fix points of the age model of Core PS92/039-2.

Depth [cmbsf]	Age [cal. ka B.P.]	Marine Isotope Stage	Fix point Origin
65	11.35	1	1
104.5	15.92	2	1
128	17.87	2	1
150	29.59	3	2
227.5	40.37	3	2
298	44.78	3	2
388	81	5.1	3
610	130	5/6 boundary	1

Origin of the age fix points: (1) correlation of carbonate content and magnetic susceptibility to nearby Core PS1533-3 (Spielhagen et al., 2004), (2) AMS radiocarbon dates, (3) occurrence of the benthic foraminifera *Pullenia bulloides*, a stratigraphic marker for event 5.1 (~81 ka) in the polar North Atlantic (Haake and Pflaumann, 1989). Note that AMS¹⁴C ages used in the age model of Core PS1533-3 were corrected for a reservoir effect of 400 years and calibrated using the CALIB 4.3 program (Spielhagen et al., 2004) and that the exact ages of the correlation tie points were calculated using linear interpolation. The ages of MIS boundaries are adopted in accordance to Lisiecki and Raymo (2005) and Thompson and Goldstein (2006).